MARTIN MARIETTA ENERGY SYSTEMS LIBRARIES
3 4456 0364247 7

CENTRAL RESEARCH LIBRARY
DOCUMENT COLLECTION

6

ORNL-3078
UC-25 - Metals, Ceramics, and Materials

X-RAY AND METALLOGRAPHIC STUDY OF THE NICKEL-RICH ALLOYS OF THE NICKEL-MOLYBDENUM SYSTEM. II

P. V. Guthrie
E. E. Stansbury

CENTRAL RESEARCH LIBRARY
DOCUMENT COLLECTION
LIBRARY LOAN COPY
DO NOT TRANSFER TO ANOTHER PERSON
If you wish someone else to see this document, send in name with document and the library will arrange a loan.

OAK RIDGE NATIONAL LABORATORY
operated by
UNION CARBIDE CORPORATION
for the
U.S. ATOMIC ENERGY COMMISSION

LEGAL NOTICE

This report was prepared as an account of Government sponsored work. Neither the United States, nor the Commission, nor any person acting on behalf of the Commission:

A. Makes any warranty or representation, expressed or implied, with respect to the accuracy, completeness, or usefulness of the information contained in this report, or that the use of any information, apparatus, method, or process disclosed in this report may not infringe privately owned rights; or

B. Assumes any liabilities with respect to the use of, or for damages resulting from the use of any information, apparatus, method, or process disclosed in this report.

As used in the above, "person acting on behalf of the Commission" includes any employee or contractor of the Commission, or employee of such contractor, to the extent that such employee or contractor of the Commission, or employee of such contractor prepares, disseminates, or provides access to, any information pursuant to his employment or contract with the Commission, or his employment with such contractor.

ORNL-3078
UC-25 – Metals, Ceramics, and Materials
TID-4500 (16th ed.)

Contract No. W-7405-eng-26

METALLURGY DIVISION

X-RAY AND METALLOGRAPHIC STUDY OF THE NICKEL-RICH ALLOYS OF THE NICKEL-MOLYBDENUM SYSTEM. II

Work performed at the
University of Tennessee
Department of Chemical and Metallurgical Engineering
under
Subcontract No. 1114

P. V. Guthrie, Graduate Student
and
E. E. Stansbury, Consultant to Metallurgy Division

DATE ISSUED
JUL - 3 1961

OAK RIDGE NATIONAL LABORATORY
Oak Ridge, Tennessee
operated by
UNION CARBIDE CORPORATION
for the
U.S. ATOMIC ENERGY COMMISSION

MARTIN MARIETTA ENERGY SYSTEMS LIBRARIES
3 4456 0364247 7

CONTENTS

Abstract 1

Introduction 2

Literature Survey 3

Experimental Procedure 6

- Alloy Preparation 6
- Preparation of Specimens for Analysis 8
- X-Ray Analysis 10
- Metallographic Technique 11
- Composition Analysis 11

Results 12

- The Phase Diagram 13
- Photomicrographs 14
- Debye-Scherrer X-Ray Patterns 23
- X-Ray Spectrometer Patterns 26
- Hardness Data 26

Discussion of Results 31

- The α Phase 31
- The β Phase — Ni_4Mo 33
  - Evidence of an Ordered Structure 35
  - Derivation of Ordered Cell 35
  - Discussion of Structure 38
- β Plus α 39
- The γ Phase — Ni_3Mo 41
- β Plus γ 42
- α Plus γ 43
- The δ Phase — NiMo 43

Conclusions 44

List of References 45

Appendix A. Correlation of Tetragonal and Cubic Indices 46

Appendix B. Hardness Data and Analysis of Debye-Scherrer X-Ray Films 48

X-RAY AND METALLOGRAPHIC STUDY OF THE NICKEL-RICH ALLOYS OF THE NICKEL-MOLYBDENUM SYSTEM. II

P. V. Guthrie E. E. Stansbury

ABSTRACT

This investigation is a continuation of previous studies on the nickel-rich alloys of the nickel-molybdenum binary alloy system. The research was conducted on alloys produced by melting and casting or by the powder metallurgy technique. Alloys ranging from 18 to 60 wt % molybdenum were prepared and homogenized in a hydrogen atmosphere at 1250°C for a minimum of 50 hr. Subsequent heat treatments in the temperature range 700 to 1000°C provided information on the progress of phase transformations in the system and, in so far as possible, indicated the equilibrium phase relationships to be expected. X-ray, metallographic, and hardness-measuring techniques were used.

The lattice parameter of the α solid solution as a function of molybdenum concentration was determined and used as an aid in establishing the extent of solid solubility of molybdenum in nickel. Molybdenum expands the nickel lattice at the approximately constant rate of 0.0033 A per weight per cent molybdenum.

The peritectoid reaction for the formation of the β phase from the α and γ phases was established at 868 ± 2°C, which compares to a previously reported temperature of 840°C. The body-centered tetragonal structure of the β phase was confirmed, although there is evidence for an intermediate structure to form during the process of transformation of the α to the β phase. The etching characteristics of the β phase were observed to be quite variable, depending on the etchant and the rate at which the β had formed from α. In general, etching tends to produce a Widmanstätten pattern presumably associated with the large number of orientations available to β as it forms.

Alloys in the composition range between the solubility limit of molybdenum in nickel and the β phase composition develop Widmanstätten structures similar to the pure β phase. For this reason it has not been possible to establish whether or not a two-phase ($\alpha + \beta$) region exists for these compositions or that a nonstoichiometric ordering is occurring.

The peritectoid reaction for the γ phase was observed at 910°C, which confirms earlier research on the present project and compares to the previously reported 890°C. The γ phase does not possess a simple close-packed hexagonal unit cell as reported in earlier literature. X-ray diffraction studies showed a large number of faint lines which could not be analyzed to provide the structure.

X-ray, metallographic, and hardness observations indicate that the α phase transforms through one or more intermediate phases in approaching the equilibrium state for the alloy. The sequence frequently involves a precipitation from the α phase, followed by a grain-boundary-nucleated growth process yielding the equilibrium phases.

INTRODUCTION

This investigation is a continuation of the study of nickel-rich alloys containing molybdenum, a subject of research of the Department of Chemical and Metallurgical Engineering of the University of Tennessee for the past several years under subcontract No. 1114 with the Union Carbide Nuclear Company.

In an effort to produce superior alloys capable of withstanding the high temperatures and corrosive atmospheres in nuclear reactors, a more extensive investigation of nickel-base alloys was begun at the Oak Ridge National Laboratory. Of the many alloying agents investigated, molybdenum in particular was outstanding in that nickel-molybdenum alloys exhibited very high resistance to chemical corrosion as well as good high-temperature properties. However, these alloys leave much to be desired where oxidation resistance is a prime consideration.

Further additions of chromium and, possibly, iron, manganese, and silicon (as found in Hastelloy B, a commercial alloy produced by the Haynes Stellite Company) were found to increase the high-temperature oxidation resistance of these nickel-molybdenum alloys, consequently giving them a much wider range of uses. But, before the effects of such additions can be understood, it is essential to have a more accurate and thorough knowledge of the binary system.

The purpose of this investigation was to conduct a program of research which would lead to a more complete understanding of the nickel-rich portion of the nickel-molybdenum equilibrium diagram. The research covered the composition range 18 to 62% molybdenum and the temperature range 600 to 1000°C.

LITERATURE SURVEY

Alloys of nickel and molybdenum have been studied rather extensively in the past, with two complete constitutional diagrams being published. The first to publish data on this system were Grube and Schlect (1), who reported the previous work of Baar (1), Dreibholz (1), and Koster and Schmidt (1) along with their own work. Baar's investigation by thermal analysis and microscopic examination was concerned with the higher-temperature region of the diagram, including the solidus and liquidus lines. Dreibholz's work essentially confirmed the previous work of Baar.

Koster and Schmidt found by hardness measurements that alloys of more than 18 wt % molybdenum show, upon "aging," an increasing hardness beginning at 600°C, with a maximum value at approximately 800°C. They also established several points showing the effect of molybdenum on the Curie temperature of nickel.

Grube and Schlect (1) sought to complete the phase diagram by electrical conductivity and hardness measurements, x-ray structure identifications, and microscopic examinations. However, they were unable to do so and reported indefinite phase boundaries in their constitutional diagram, as shown by Fig. 1. Their region in question exists below 880°C and extends from approximately 31 to 62 wt % molybdenum. They reported evidence of

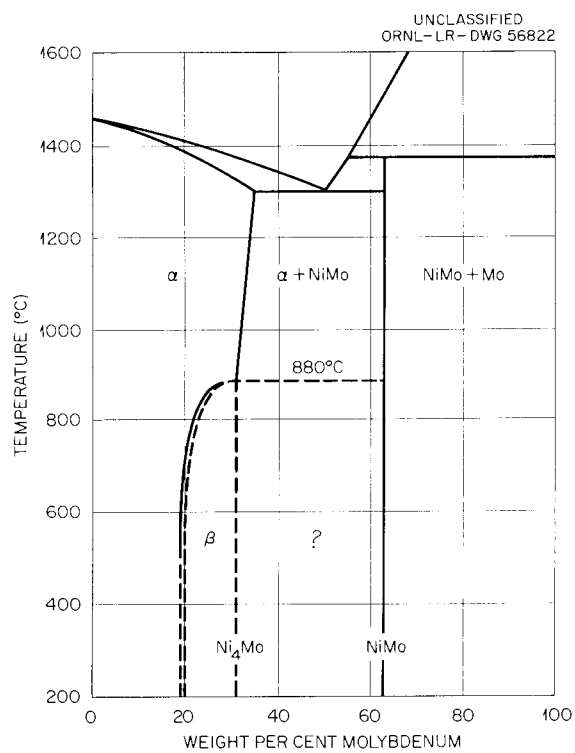

Fig. 1. Nickel-Molybdenum Constitutional Diagram. After Grube and Schlect (1).

a second phase existing in this region but were unable to identify it. However, they did determine the structure of the β phase, corresponding to the compound Ni_4Mo, as face-centered tetragonal with a c/a ratio of 0.986. They further reported and gave evidence for ordering reactions in this region.

They also reported solid solution lattice spacings for several alloys which had been annealed at 1100°C and quenched. These are shown in Fig. 2, plotted as a function of their corresponding weight per cent molybdenum.

A continuation of this work was performed by Grube and Winkler (2). Their principal contribution to the constitutional diagram, as shown by Fig. 3, was the determination of the previously questionable phase occurring in the range from about 31 to 62% molybdenum. They identified this new phase, γ, corresponding to the compound Ni_3Mo, as having a hexagonal close-packed structure with a c/a ratio of 1.65.

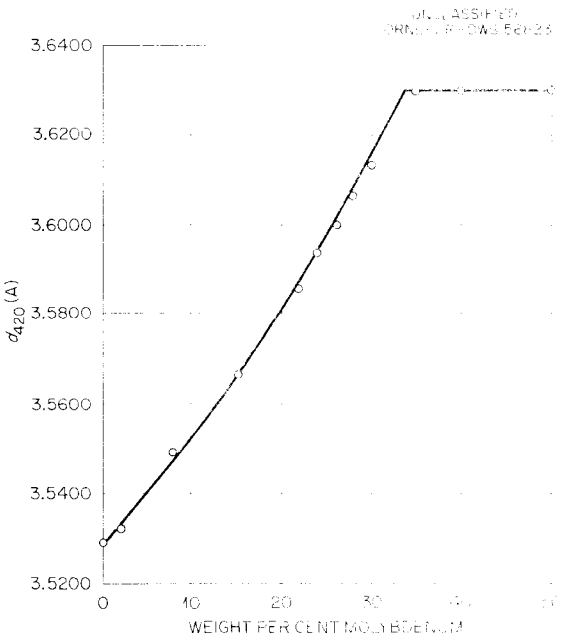

Fig. 2. Plot of (420) Lattice Spacings as a Function of Weight Per Cent Molybdenum, as Determined by Grube and Schlect (1). Alloys were annealed at 1100°C and quenched.

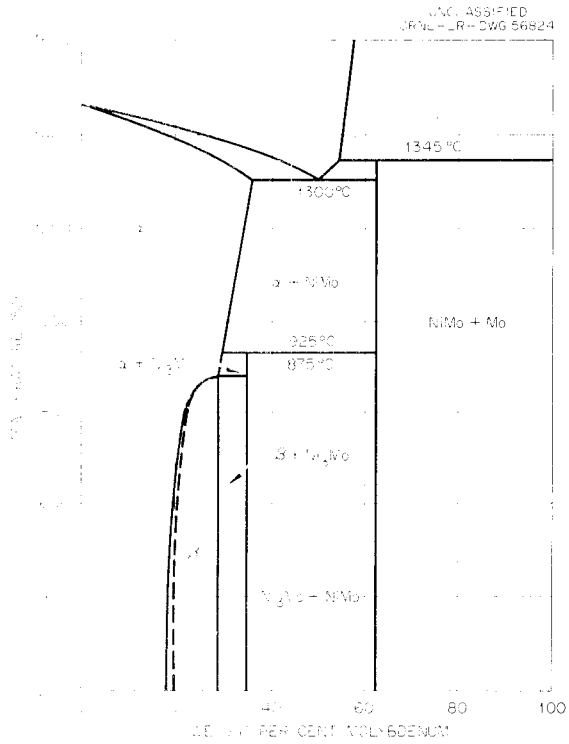

Fig. 3. Nickel-Molybdenum Constitutional Diagram. After Grube and Winkler (2).

The second complete constitutional diagram was later published by Ellinger (3), as shown by Fig. 4. The major difference between this diagram and that of Grube and Winkler, outside of slight variations in transformation temperatures and phase boundaries, was the interpretation of the β phase. Ellinger's interpretation, supported mainly by x-ray, metallographic, and age-hardening data, was that the β phase resulted from a peritectoid reaction involving α and γ. His x-ray work did not reveal the structure of the β phase, but he did confirm the previous conclusions regarding the γ phase.

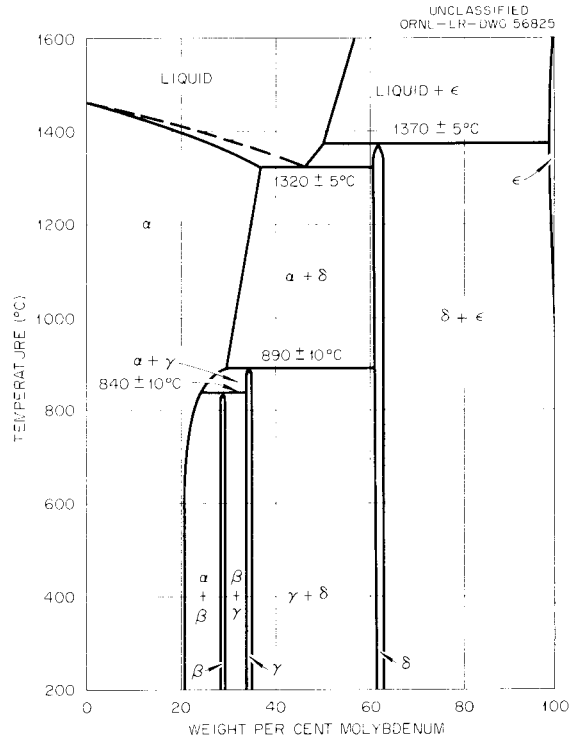

Fig. 4. Nickel-Molybdenum Constitutional Diagram. After Ellinger (3).

The crystal structure of Ni_4Mo was investigated by Harker (4), who reported that an alloy containing about 20 at. % molybdenum undergoes an ordering reaction below 840°C which results in a slight tetragonal distortion of the cubic lattice. He described this new cell, containing 2.5 times the volume of the distorted face-centered cubic cell, as a $C_{4h}^{5}-I\frac{4}{m}$ space group with the dimensions of the unit cell being: a_0 = 5.720 A, c_0 = 3.564 A, and c/a = 0.6231. His conclusions were based on x-ray diffraction studies of a 27.3 wt % molybdenum alloy that possessed a face-centered cubic structure having a lattice parameter a_0 = 3.612 A upon quenching from 1200°C.

An investigation of the nickel-molybdenum-chromium ternary system about 1250°C by Grant and Bloom (5) led to several changes in that region of the nickel-molybdenum binary diagram. These were essentially a correction for the eutectic composition and a correction for the δ-peritectic temperature, along with the necessary changes in the liquidus curve as shown by Fig. 5.

The most recent investigation of the nickel-molybdenum system was performed by Stoffel (6) on alloys of 20 to 33% molybdenum, using metallographic and x-ray techniques. He observed that the complete range of alloys investigated, with the exception of a 20 wt % alloy, readily responded to heat treatment, producing Knoop hardnesses between 350 and 550. In the 22 to 25% molybdenum range, structures corresponding to typical precipitation reactions were observed to develop, while in the 27 to 33% molybdenum alloys a tendency to form lamellar structures was observed.

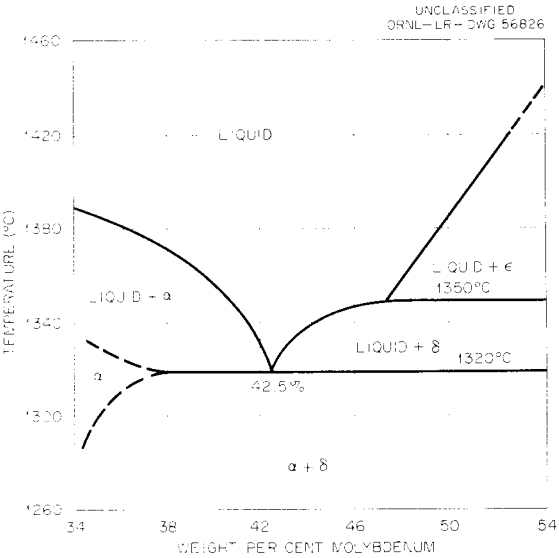

Fig. 5. Central Region of Nickel-Molybdenum Diagram. After Grant and Bloom (5).

With existing x-ray techniques he was unable to establish the formation or structure of the β phase. However, he did observe and agree with the previously published data on the γ phase. In general his data supported the basic features of the diagram reported by Ellinger (3), with the exception of the temperature limits of the α-γ region. Stoffel observed these upper and lower temperature limits to be approximately 900 and 875°C, respectively.

EXPERIMENTAL PROCEDURE

Alloy Preparation

The seven alloys which had been previously prepared and used by Stoffel (6) were also used initially in this investigation. However, repeated inconsistencies in both x-ray data and metallographic examinations were observed, indicating that possibly some inhomogeneity still existed in these furnace-cooled ingots even though they had been homogenized at 1250–1300°C for 100 hr or more. Thus, these specimens were soon abandoned and a completely new series of alloys prepared.

The preparation of these new alloys utilized two markedly different metallurgical techniques. Induction melting and chill casting under a partial vacuum was employed to produce the dense homogeneous specimens necessary for microscopic examination, while powder metallurgical techniques were used for the preparation of alloys to be used solely for x-ray analysis.

Nickel of 99.95% purity, supplied by the International Nickel Company, and molybdenum of 99.8% purity, supplied by the Climax Molybdenum Company, were used in the preparation of the melts. The weighed stock of approximately 250 g was placed in a high-purity alumina crucible surrounded by a graphite liner. A hydrogen atmosphere surrounded the metal while melting and holding in the molten state, but a partial vacuum of approximately 25 in. Hg was obtained in the system before casting. Prior to casting, the molten metal was superheated 300 to 400°F for 30 to 45 min to ensure a completely homogeneous melt. The molten metal was chill cast into a cold copper mold, producing ingots 3/4 in. wide by 1/2 in. thick by approximately 3 in. long.

Metallographic examination of the as-cast ingots revealed fairly dense alloys with some dendritic segregation, but no observable mass segregation (Fig. 6). After homogenization for 100 hr at 1250°C the alloys appeared to be metallographically homogeneous (Fig. 7).

For most purposes in this investigation, the alloys were reduced 10 to 50% in thickness by hot rolling. Alloys of molybdenum content up to 25 wt % were reduced readily 50% or more, while alloys in the 28 to 31% range developed cracks, chiefly at the grain boundaries, upon reducing 8 to 10%. A gradual increase in the amount of permissible reduction was observed in the 32 to 39% range, with a maximum of 30% reduction attained in the 39% alloy. All hot rolling was done at temperatures between 1000 and 1150°C.

A subsequent anneal for 50 hr at 1250°C produced in most cases a coarse-grained α matrix, as shown by Fig. 8.

Hydrogen-reduced high-purity metal powders screened through 325 mesh were used in the preparation of the alloys intended for x-ray analysis. The powders, accurately weighed in the desired proportions, were thoroughly mixed by tumbling on slowly turning rollers for approximately 100

hr. From these mixtures, disks of 1/2 in. diameter and 1/8 in. thickness were pressed at 60 tons/in.^{2} followed by a 100-hr sintering period at 1250–1300°C in hydrogen. If the resulting sintered disk was sufficiently ductile, it was given a 50% reduction by cold rolling and then was resintered for another 100 hr. Such a reduction was not permissible in some of the alloys, with the same general trend existing as previously indicated in the hot rolled ingots.

Microscopic and x-ray examinations revealed that these alloys were homogeneous though still having considerable porosity (Fig. 9).

Preparation of Specimens for Analysis

Specimens intended for metallographic examination were cut from the annealed ingots to a size approximating 1/4 in. square by 3/16 in. thick. Prior to heat treatment, the specimens were placed in Vycor capsules which were then evacuated to a pressure of 10–15 μ Hg and sealed. Similarly, x-ray specimens in the form of filings taken from the sintered disks were sealed in Vycor capsules.

Heat treatments below 1000°C were carried out in horizontal-type tube furnaces wound with Nichrome. Temperature gradients were minimized by using long tubes with small diameters (36 in. long, 2-1/2 in. in diameter) and decreasing the spacing between windings at each end of the tube. Plugs in both ends eliminated external air currents. Above 1000°C a furnace using Globar-type heating elements was used.

All furnaces were controlled by separate Leeds and Northrup Micromax potentiometers equipped with time-duration-adjusting-type controls in response to Chromel-Alumel thermocouples. A maximum temperature variation of ±3°C was observed for heat treatments extending into hundreds of hours, while ±1°C was normally realized on heat treatments of 50 hr or less.

Temperature measurements were made with a 22-gage platinum vs platinum–10% rhodium thermocouple. The thermocouple was initially calibrated at the aluminum point and at the gold point and, later, during the course of the investigation, recalibrated at the gold point. All calibration points were within 0.5°C of the accepted value of the standard.

UNCLASSIFIED
PHOTO 53654

Fig. 6. 27% Molybdenum Alloy, as Cast. Induction melted and chill cast.

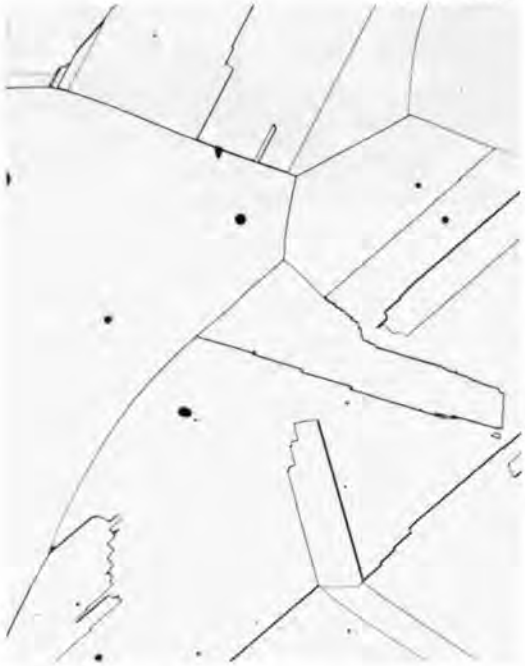

Fig. 7. 27% Molybdenum Alloy, Homogenized 100 hr at 1250°C. Induction melted and chill cast.

Fig. 8. 27% Molybdenum Alloy, Homogenized 100 hr at 1250°C, Followed by Rolling and Additional Anneal for 50 hr at 1250°C. Induction melted and chill cast.

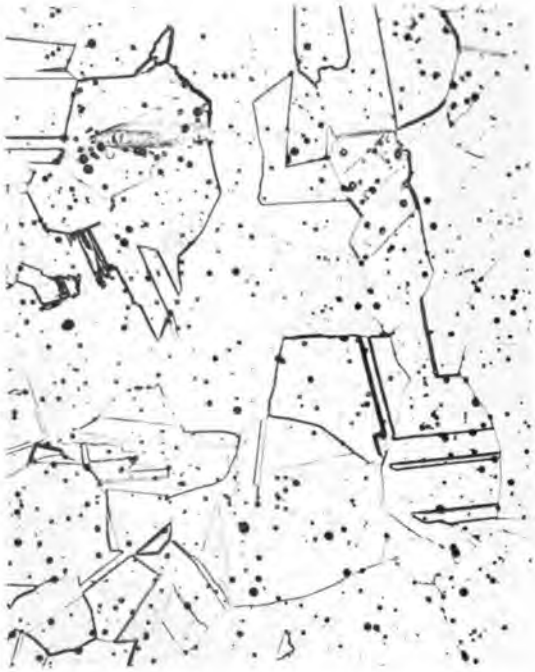

Fig. 9. 18% Molybdenum Alloy Made by Powder Metallurgical Process. Pressed at 60 tons/in.^{2}; sintered 100 hr at 1250–1300°C.

Maximum temperature variations for each heat treatment were determined and recorded along with numerous readings throughout the course of the heat treatment. The calibrated couple was always inserted prior to a temperature measurement and removed thereafter to reduce, if possible, any alteration of the calibration.

X-Ray Analysis

The majority of the x-ray data were obtained by conventional methods, employing powdered specimens. For this analysis Debye-Scherrer cameras having radii of 5.73 cm were used, utilizing nickel-filtered copper radiation producing a characteristic wavelength of 1.54050 A ($K\alpha_1$).

Specimens 10 to 20 mils in diameter were prepared by either rolling the heat treated and screened powders (200 mesh) into filaments, using cellulose acetate cement as an adhesive, or by coating a cylindrical layer of the powder-cement mixture on the surface of a small glass fiber. The former method was preferred by the author because shorter exposure times were realized.

All film measurements were made on a fluorescent indexing apparatus capable of determining each line position within ±0.002 in., thus realizing an accuracy of ±0.0003 A for each lattice-parameter determination. Typical film-shrinkage corrections were made by using a method described by Buerger (7). Lattice parameters were determined by extrapolation of the plot of the apparent parameter as a function of

$$1/2 \left(\frac{\cos^2 \theta}{\sin^2 \theta} + \frac{\cos^2 \theta}{\theta} \right)$$

to its intercept with the ordinate. In this function, θ is the Debye diffraction angle.

In some instances it was found desirable to resolve regions containing numerous diffraction lines by means of a powder diffractometer capable of traversing a 2θ of 180° with angular velocities of 1/4 and 1/8° per minute. Additional correlation of metallographic with x-ray data was obtained by running similar diffractometer traces on metallographic specimens.

Metallographic Technique

The heat treated specimens intended for microscopic examination were mounted in Lucite prior to polishing. The usual polishing procedures then followed, with the final polish being done by Linde B on a microcloth.

In general, an echant made up of two parts of 20% hydrochloric acid plus one part hydrogen peroxide, applied hot with a swab, was satisfactory in revealing the microstructure of the entire composition range studied. Alloys containing a β precipitate in an α matrix revealed the fine β structure most favorably by a similar application of an etchant composed of one part 10% chromic acid plus one part 50% hydrochloric acid, following a light hydrochloric acid–hydrogen peroxide etch.

Microhardness measurements were subsequently made on all metallographic specimens by using a Tukon tester equipped with a diamond pyramid hardness indenter. An average of several indentations was used to compute the reported hardness.

Composition Analysis

The fact that molybdenum has a very marked effect on the lattice parameter of nickel provided a convenient means of analyzing the molybdenum content of the vacuum cast alloys. Precise α lattice parameters for the powder metallurgy specimens were determined and plotted as a function of their accepted weight per cent molybdenum (Fig. 10). By use of this plot as a standard, similar lattice parameter measurements of the vacuum cast alloys yielded their apparent molybdenum content. Unfortunately, the range of this analysis is limited by the solubility of molybdenum in nickel, which was found to be approximately 37% at 1250°C.

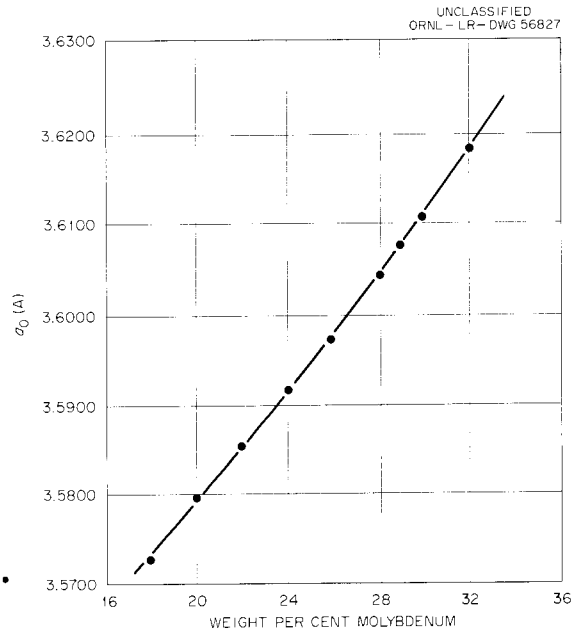

Fig. 10. α Lattice Parameter Plot. Values are given in Table B-1 in Appendix B.

RESULTS

A series of 29 specimens representing 23 different molybdenum concentrations were prepared by two different techniques and used during this investigation. In the initial stages of the investigation powder metallurgy specimens were used for both metallographic and x-ray analysis. As work progressed, it became apparent that structure identification by microscopic examination would be greatly facilitated if much of the retained porosity in these powder compacts could be eliminated. It was found that this could be done by repeatedly cold working and annealing the specimens, involving much time and labor, as well as increasing the possibility of further contamination. At this stage of the investigation, work was concentrated on the development of casting equipment and techniques through which dense, homogeneous bulk specimens necessary for good metallographic work could be prepared. These efforts were successful, and, consequently, powder specimens were used solely for Debye-Scherrer powder patterns. A more complete description of the techniques and procedures used in the alloy development is given in the preceding section, "Experimental Procedure."

The vacuum cast alloys, analyzed by the previously discussed technique, were all found to lie within experimental error of their expected positions on the standard parameter plot. Since they were used only in estimating phase boundaries by metallographic methods, no corrections for molybdenum content were made. The following is a list of alloys prepared by the indicated methods.

Powder Metallurgy Alloys (wt % molybdenum)		Vacuum Cast Alloys (wt % molybdenum)	
18.00	30.00	18.7	31
20.00	32.01	21	32
22.01	34.02	23	33
24.02	35.27	25	34
26.01	36.00	27	35
27.98	38.01	28	36
29.00	62.01	29	39
		30	

During this investigation some 200 Debye-Scherrer powder patterns were made and analyzed for structures and parameters. Supporting these

powder photograms were approximately 160 metallographic specimens, all of which were examined microscopically, photographed, and analyzed by an x-ray spectrometer. In addition to these analyses, microhardness measurements were made on many of these bulk specimens.

In this section the results of these analyses are given in the form of a proposed phase diagram, supported by microstructures, x-ray patterns, and hardness measurements. These data are presented in separate sections in order to provide a convenient means by which the results of future studies may be compared with those of this experiment.

The Phase Diagram

The data obtained in this investigation, primarily through pertinent x-ray and metallographic analyses, led to a proposed partial phase diagram for the nickel-rich portion of the nickel-molybdenum system. In general these data support the basic form of Ellinger's constitutional diagram (3), although several changes are proposed. Diagrammatically, these can be seen by comparing Fig. 11 with Fig. 3, the latter being a reproduction of Ellinger's diagram as shown in the American Society for Metals Handbook.

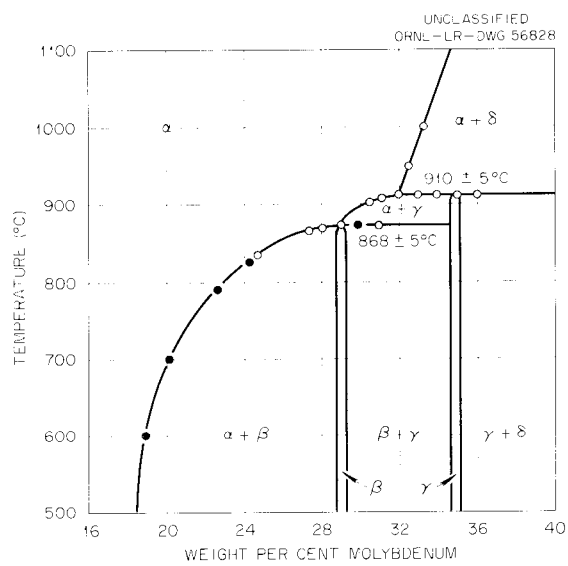

Fig. 11. Proposed Partial Diagram for the Nickel-Molybdenum Alloy System. Closed circles refer to x-ray parameter determinations; open circles refer to estimates based on metallography.

It can be seen in Fig. 11 that the β peritectoid temperature has been placed at approximately 868°C; this differs from Ellinger's value of about 840°C. Another change has been the establishment of the γ peritectoid temperature at approximately 910°C, as compared with Ellinger's value of about 890°C. Also consistent with these temperature changes were changes in the solubility limits of molybdenum in nickel in the temperature range of 800 to 900°C. The α phase boundary established by this research supports earlier observations reported by Grube and Winkler (2) (Fig. 3).

Photomicrographs

In order to conserve space only a fraction of the photomicrographs obtained in this investigation are included here. They cover the entire range of compositions and temperatures studied and are representative of the structures present. The numbered circles within the phase diagram shown in Fig. 12 refer to these photomicrographs and show their relative positions in the diagram. For example, the circled number 1 refers to the photomicrograph shown in Fig. 12-1, No. 2 refers to the photomicrograph shown in Fig. 12-2, etc.

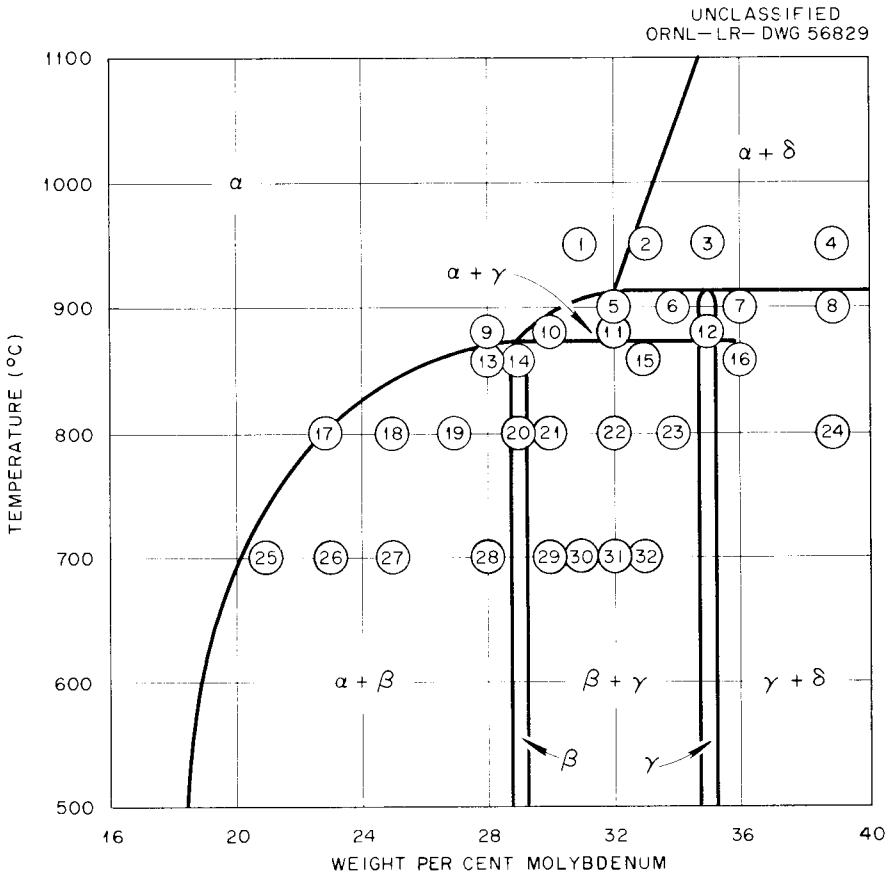

Fig. 12. Proposed Phase Diagram Showing Relative Positions of Photomicrographs Shown in Figs. 12-1 through 12-32. Circled numbers refer to the figures in this sequence.

UNCLASSIFIED
PHOTO 53655

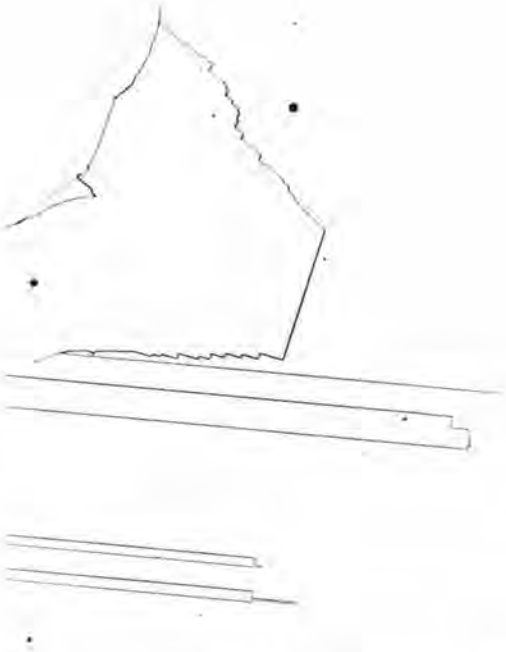

Fig. 12-1. 31% Molybdenum. 100 hr at 952°C; typical large-grained α. 200X.

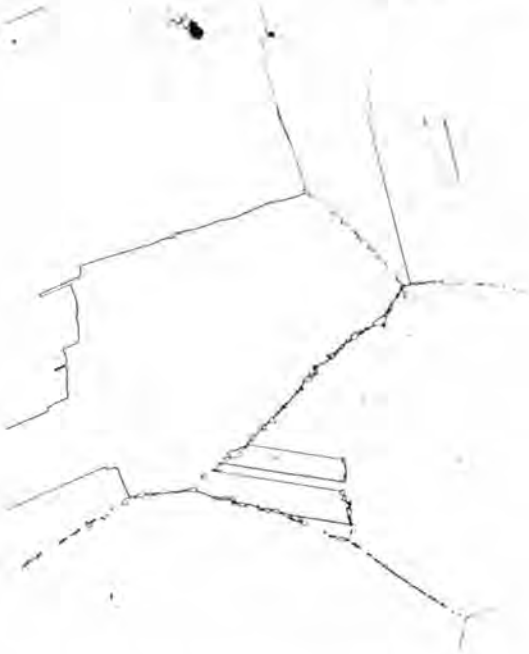

Fig. 12-2. 33% Molybdenum. 100 hr at 952°C; δ precipitate in α matrix. 200X.

Fig. 12-3. 35% Molybdenum. 100 hr at 952°C; δ in α matrix. 200X.

Fig. 12-4. 39% Molybdenum. 100 hr at 952°C; pro-eutectic α plus δ. 200X.

UNCLASSIFIED
PHOTO 53656

Fig. 12-5. 32% Molybdenum. 230 hr at 900°C; γ precipitate in α matrix. 200X.

Fig. 12-6. 34% Molybdenum. 230 hr at 900°C; $\gamma + \alpha$. 200X.

Fig. 12-7. 36% Molybdenum. 230 hr at 900°C; γ plus trace of δ. 200X.

Fig. 12-8. 39% Molybdenum. 230 hr at 900°C; $\gamma + \delta$. 200X.

UNCLASSIFIED
PHOTO 53657

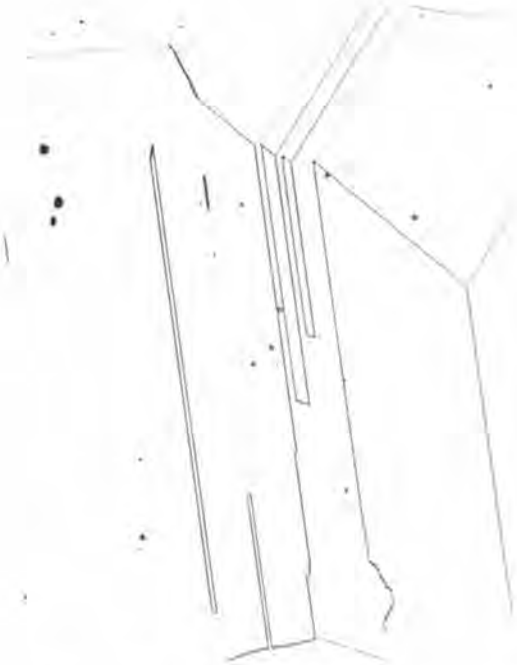

Fig. 12-9. 28% Molybdenum. 150 hr at 872°C; α showing twins. 200X.

Fig. 12-10. 30% Molybdenum. 150 hr at 872°C; γ precipitating in α matrix. 200X.

Fig. 12-11. 32% Molybdenum. 150 hr at 872°C; massive formation of $\gamma + \alpha$. 200X.

Fig. 12-12. 35% Molybdenum. 150 hr at 872°C; primary γ plus residual δ. 200X.

UNCLASSIFIED
PHOTO 53658

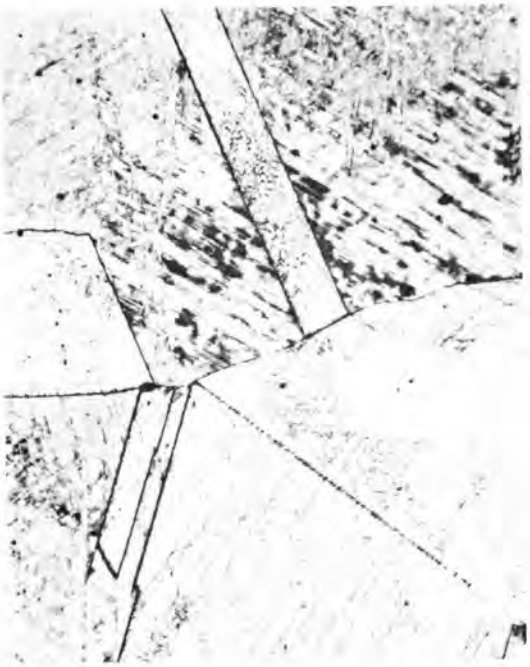

Fig. 12-13. 28% Molybdenum. 150 hr at 865°C; β in α. 200X.

Fig. 12-14. 29% Molybdenum. 150 hr at 865°C; primary β. 200X.

Fig. 12-15. 33% Molybdenum. 150 hr at 865°C; formation of $\beta + \gamma$. 200X.

Fig. 12-16. 36% Molybdenum. 150 hr at 865°C; $\gamma + \delta$ precipitate. 200X.

UNCLASSIFIED
PHOTO 53659

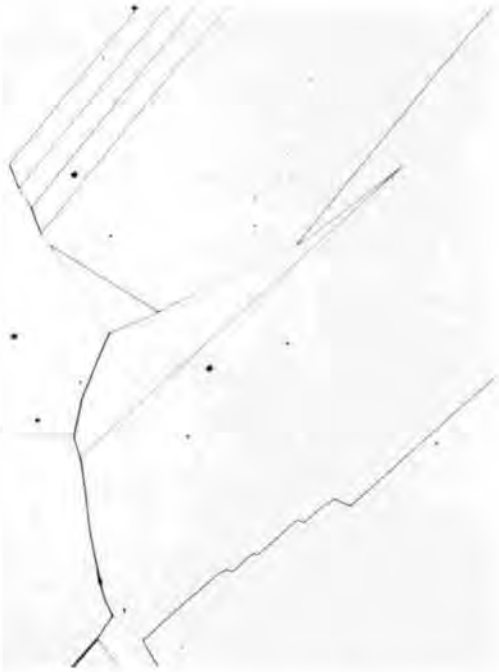

Fig. 12-17. 23% Molybdenum. 250 hr at 800°C; primary α. 200X.

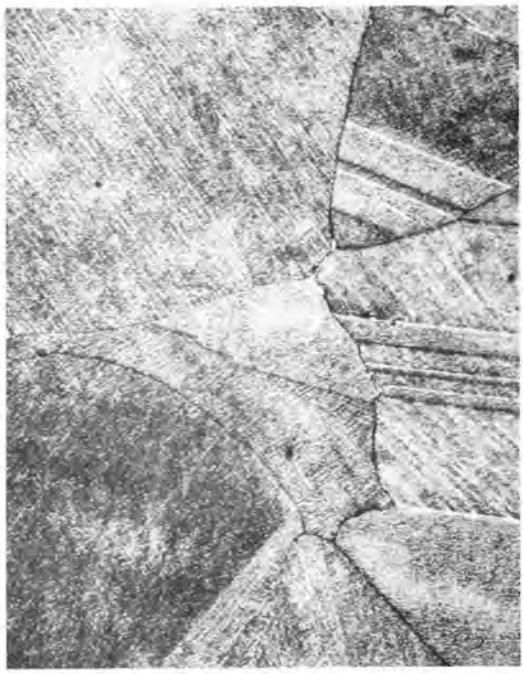

Fig. 12-18. 25% Molybdenum. 250 hr at 800°C; fine β formation in α. 200X.

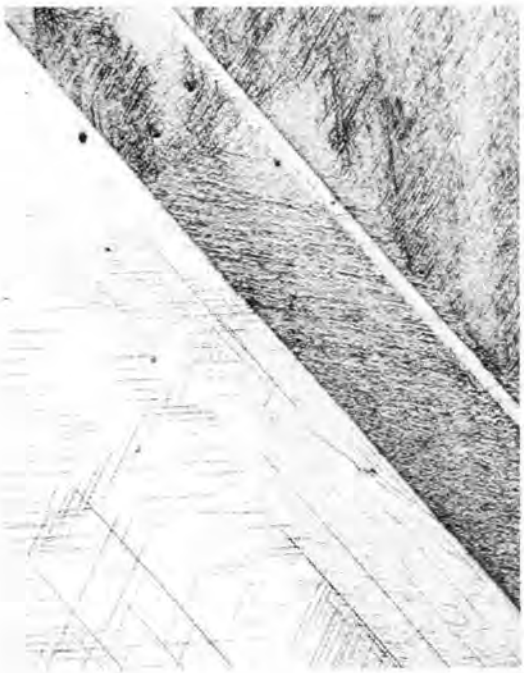

Fig. 12-19. 27% Molybdenum. 250 hr at 800°C; β in α. 200X.

Fig. 12-20. 29% Molybdenum. 250 hr at 800°C; primary β. 200X.

UNCLASSIFIED
PHOTO 53660

Fig. 12-21. 30% Molybdenum. 250 hr at 800°C; precipitate of $\beta + \gamma$. 200X.

Fig. 12-22. 32% Molybdenum. 250 hr at 800°C; $\beta + \gamma$. 200X.

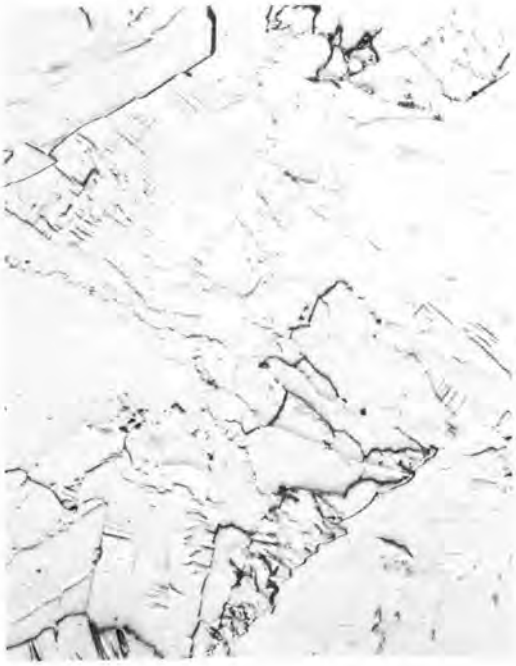

Fig. 12-23. 34% Molybdenum. 250 hr at 800°C; γ plus trace of β. 200X.

Fig. 12-24. 39% Molybdenum. 250 hr at 800°C; $\gamma + \delta$. 200X.

UNCLASSIFIED
PHOTO 53661

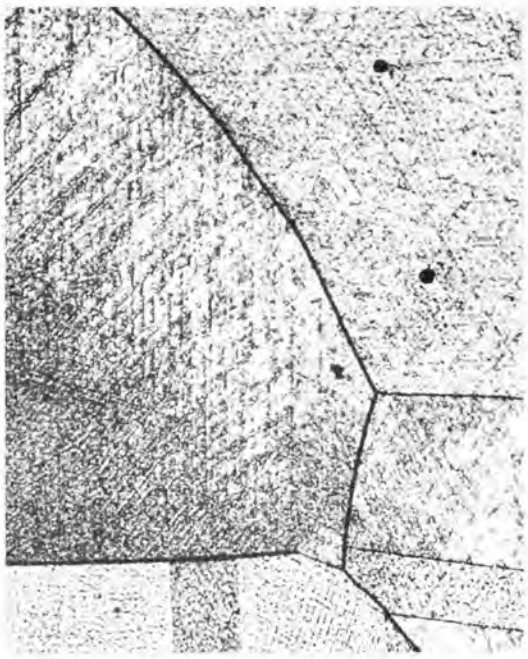

Fig. 12-25. 21% Molybdenum. 500 hr at 700°C; β in α. 200X.

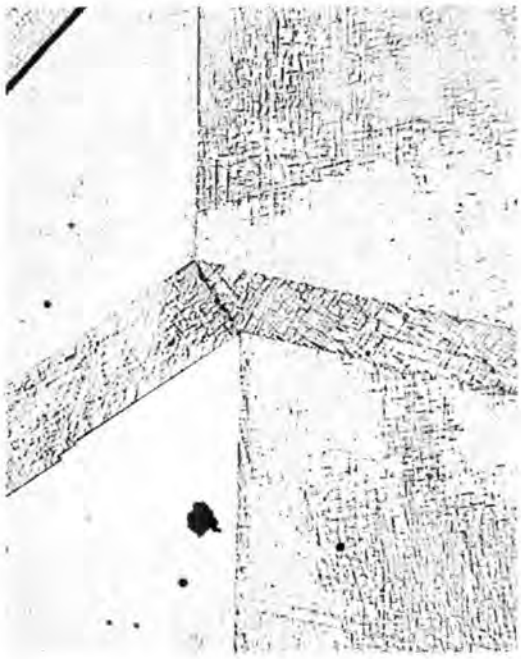

Fig. 12-26. 23% Molybdenum. 500 hr at 700°C; β in α. 200X.

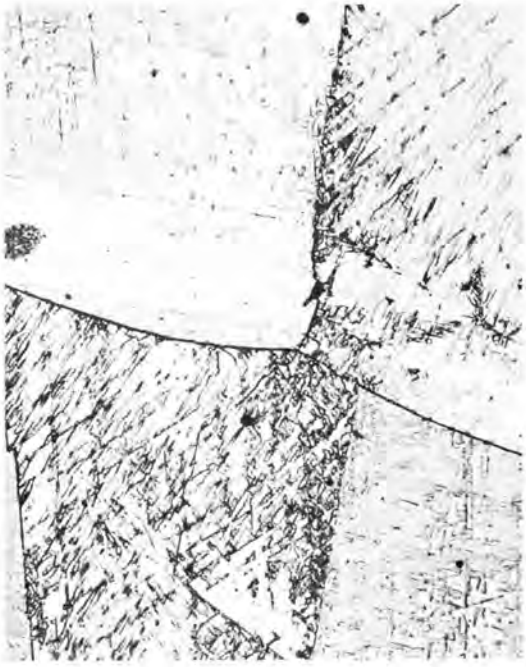

Fig. 12-27. 25% Molybdenum. 500 hr at 700°C; coarse β in α. 200X.

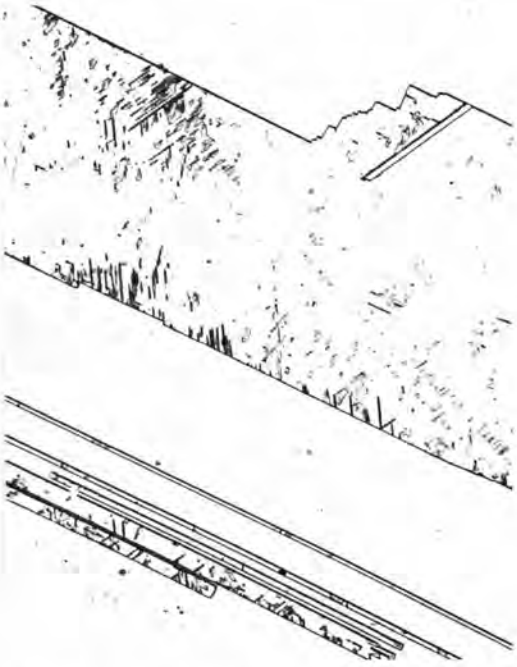

Fig. 12-28. 28% Molybdenum. 500 hr at 700°C; primarily β plus some α. 200X.

UNCLASSIFIED
PHOTO 53662

Fig. 12-29. 30% Molybdenum. 500 hr at 700°C; nucleation and growth of $\beta + \gamma$. 200X.

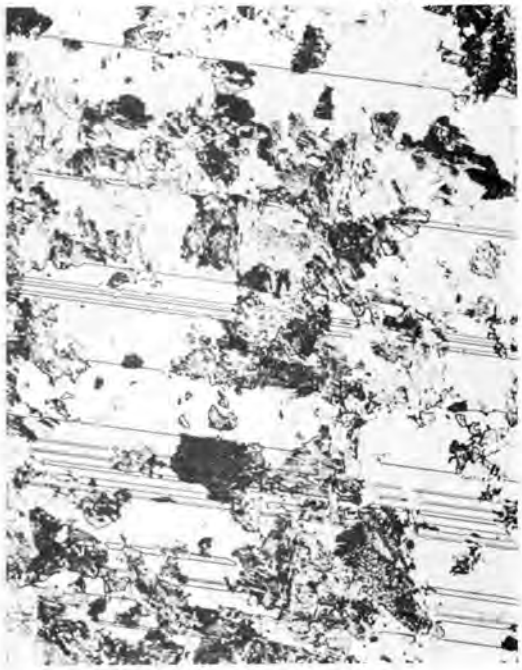

Fig. 12-30. 31% Molybdenum. 500 hr at 700°C; nucleation and growth of $\beta + \gamma$. 200X.

Fig. 12-31. 32% Molybdenum. 500 hr at 700°C; $\beta + \gamma$. 200X.

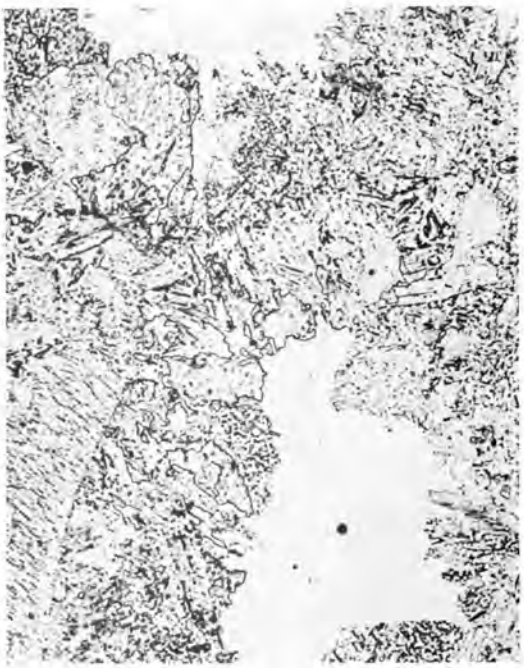

Fig. 12-32. 33% Molybdenum. 500 hr at 700°C; $\beta + \gamma$. 200X.

Debye-Scherrer X-Ray Patterns

The Debye-Scherrer x-ray photograms included here are prints from the original powder patterns, showing typical diffraction patterns observed in this system. These are unretouched and are representative of the line intensity observations made on the actual films. The photograms are shown in Figs. 13-1 through 13-4, 14-1 through 14-4, and 15-1

UNCLASSIFIED
PHOTO 53663

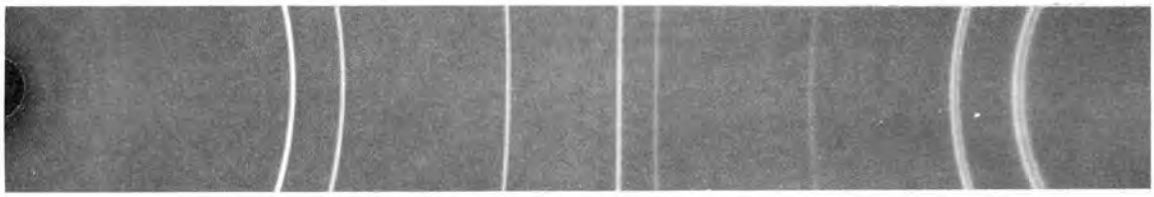

Fig. 13-1. Powder Pattern of FCC Solid-Solution Alloy, 18% Molybdenum. Heat treated at 1000°C for 64 hr.

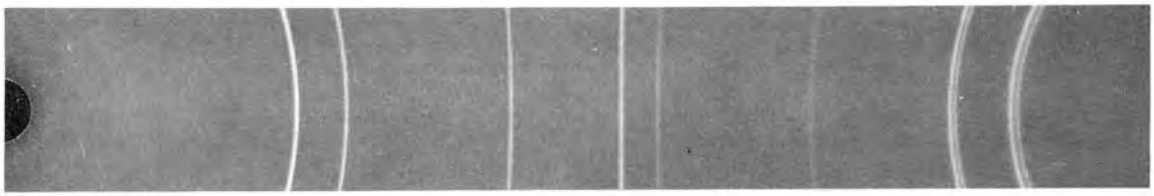

Fig. 13-2. Powder Pattern of FCC Solid-Solution Alloy, 22% Molybdenum. Heat treated at 1000°C for 48 hr.

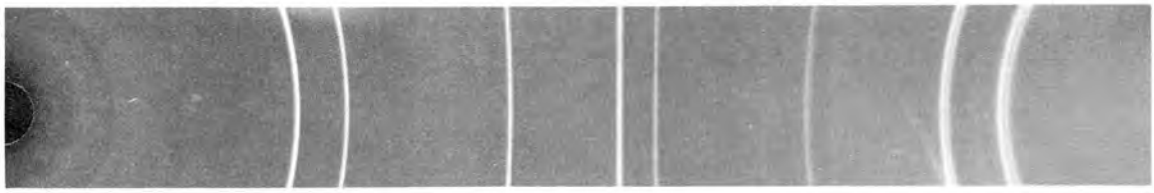

Fig. 13-3. Powder Pattern of FCC Solid-Solution Alloy, 28% Molybdenum. Heat treated at 1000°C for 48 hr.

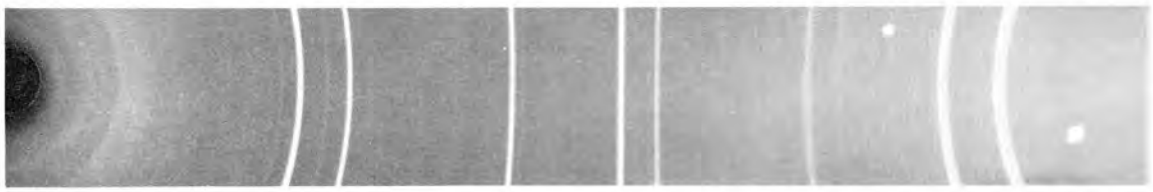

Fig. 13-4. Powder Pattern of FCC Solid-Solution Alloy, 32% Molybdenum. Heat treated at 1000°C for 36 hr.

UNCLASSIFIED
PHOTO 53664

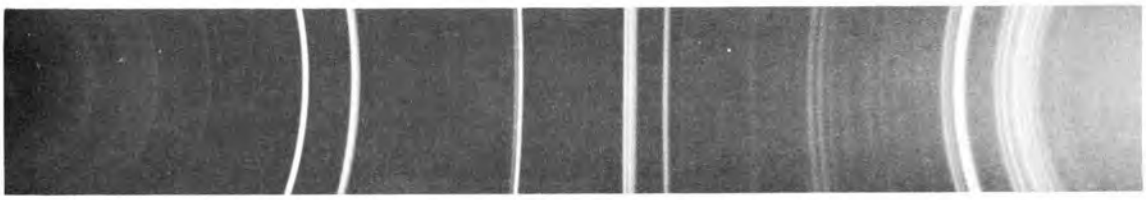

Fig. 14-1. Powder Pattern of 28% Molybdenum Alloy, Showing $\beta + \alpha$. Heat treated at 830°C for 142 hr.

Fig. 14-2. Powder Pattern of 29% Molybdenum Alloy, Showing Predominantly All β. Heat treated at 825°C for 46 hr.

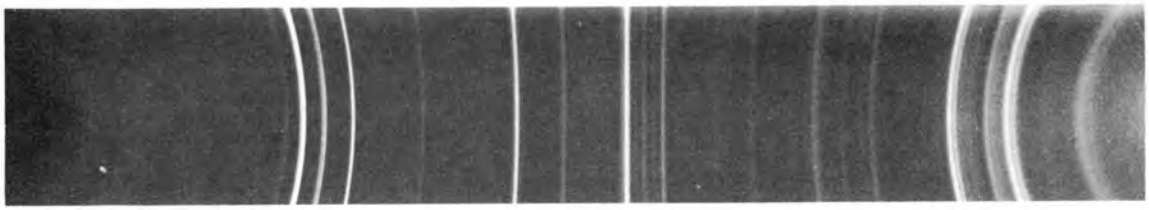

Fig. 14-3. Powder Pattern of 32% Molybdenum Alloy, Showing $\alpha + \gamma$. Heat treated at 872°C for 67 hr.

Fig. 14-4. Powder Pattern of 32% Molybdenum Alloy, Showing $\beta + \gamma$. Heat treated at 833°C for 94 hr.

UNCLASSIFIED
PHOTO 53665

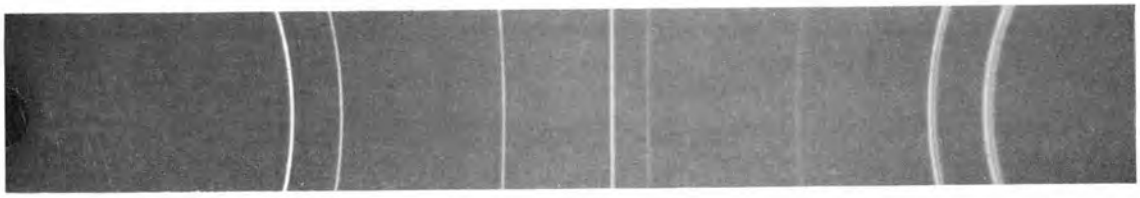

Fig. 15-1. Powder Pattern of 35% Molybdenum Alloy, Showing α plus a Trace of δ. Heat treated at 912°C for 47 hr.

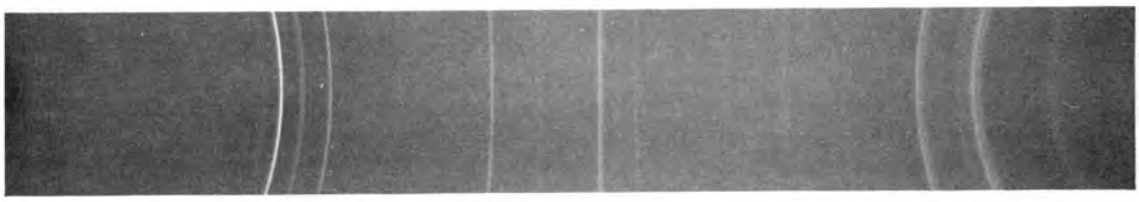

Fig. 15-2. Powder Pattern of 35% Molybdenum Alloy, Showing $\alpha + \gamma$. Heat treated at 907°C for 36 hr.

Fig. 15-3. Powder Pattern of 35% Molybdenum Alloy, Showing Predominantly All γ. Heat treated at 846°C for 90 hr.

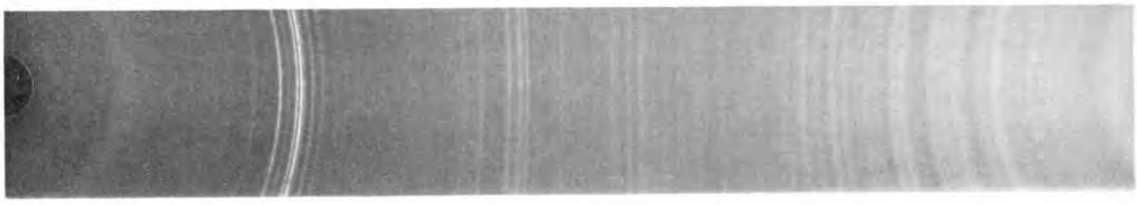

Fig. 15-4. Powder Pattern of 62% Molybdenum Alloy, Showing δ Structure. Heat treated at 851°C for 146 hr.

X-Ray Spectrometer Patterns

The typical spectrometer traces included here as Figs. 16, 17, and 18 are photographs of the actual traces. These were made from the polished metallographic specimens and were very useful in correlating the observed microstructures with the Debye-Scherrer data. In some cases spectrometer traces are omitted because preferred orientation resulting from hot rolling obscured several of the diffraction peaks. This was especially true in alloys of lower molybdenum content which contained primarily all α, and consequently in those which contained α plus β, the β being essentially ordered α.

Hardness Data

Microhardness measurements were made on many of the aforementioned metallographic specimens. These data have been plotted in Figs. 19 through 24 to show the trends in hardness as functions of time, temperature, and molybdenum concentration. Table B-1 (Appendix B) gives these values.

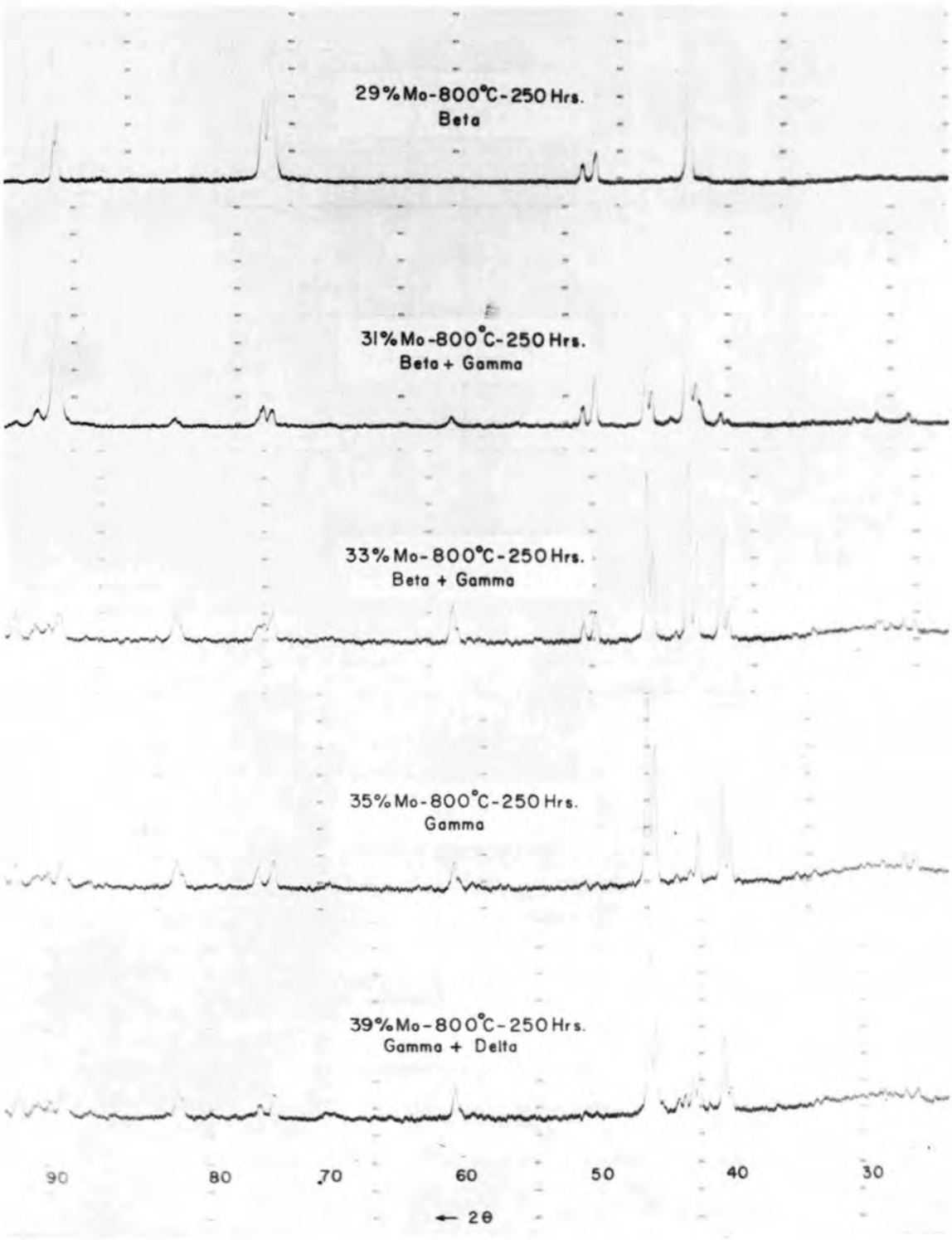

Fig. 16. X-Ray Diffractometer Traces, Showing Various Phases.

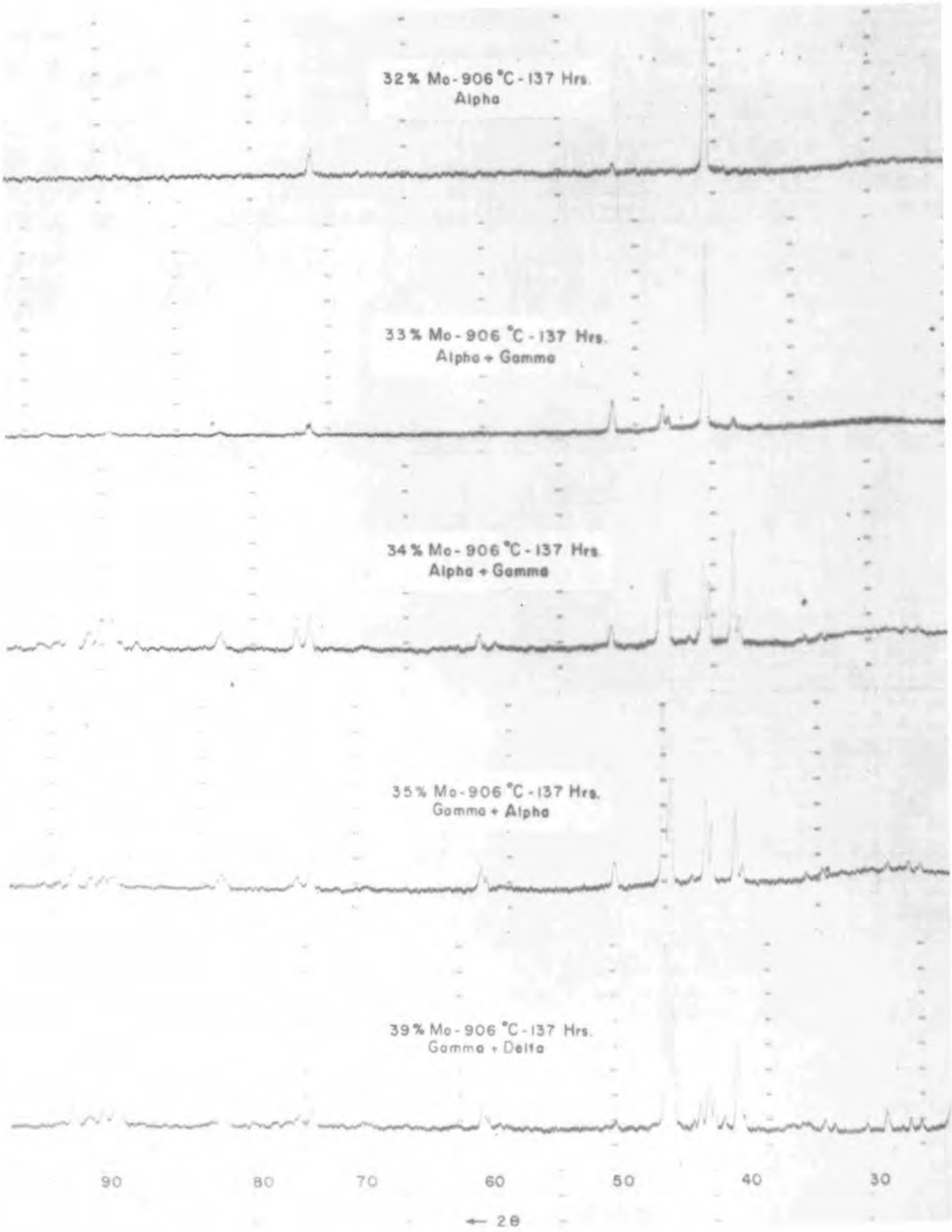

Fig. 17. X-Ray Diffractometer Traces, Showing Various Phases.

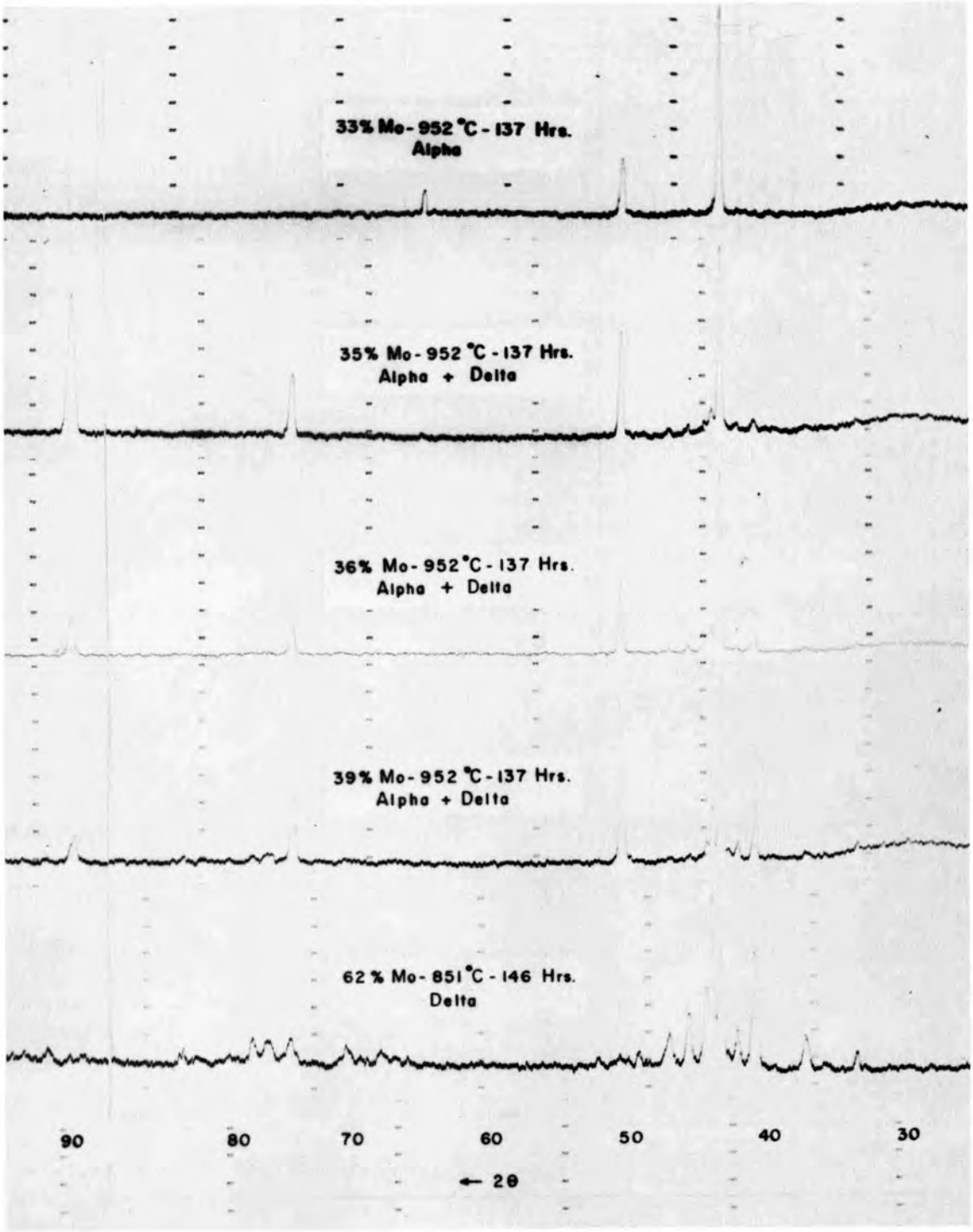

Fig. 18. X-Ray Diffractometer Traces, Showing Various Phases.

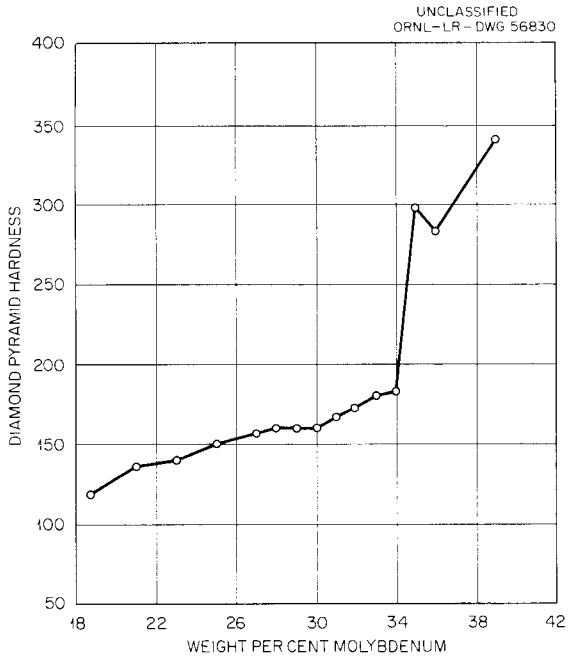

Fig. 19. Effect of Molybdenum Concentration on Diamond Pyramid Hardness of Specimens Quenched from 1000°C. Specimens were held at 1000°C for 17 hr.

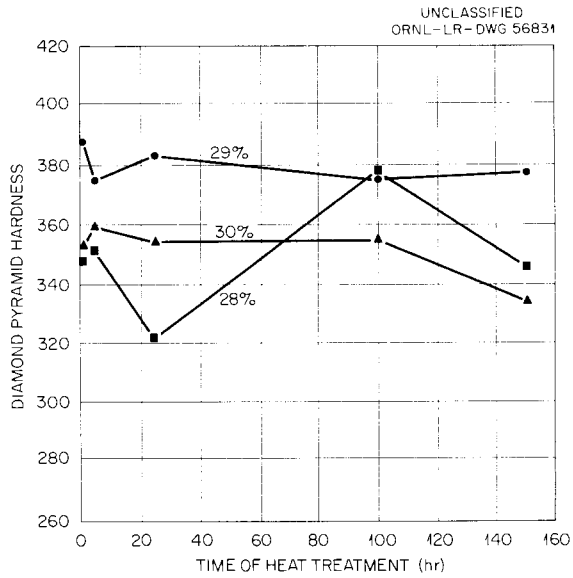

Fig. 20. Effect of Composition and Time of Heat Treatment on Hardness of 28, 29, and 30 wt % Molybdenum Alloys Aged at 865°C. As-quenched hardness shown in Fig. 19.

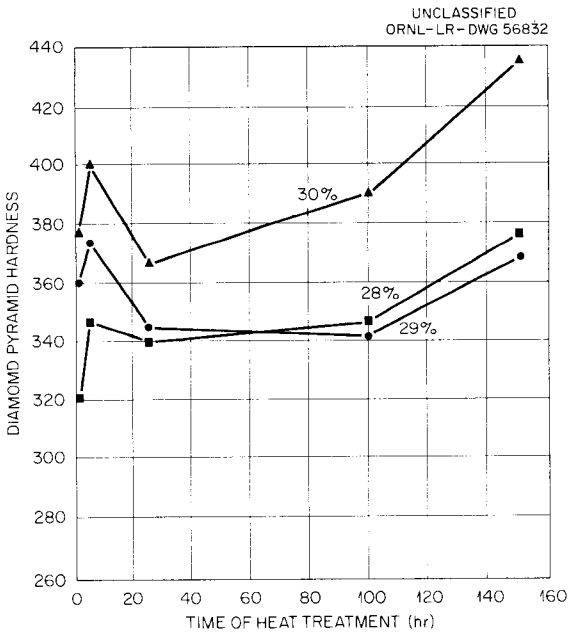

Fig. 21. Effect of Composition and Time of Heat Treatment on Hardness of 28, 29, and 30 wt % Molybdenum Alloys Aged at 825°C. As-quenched hardness given in Fig. 19.

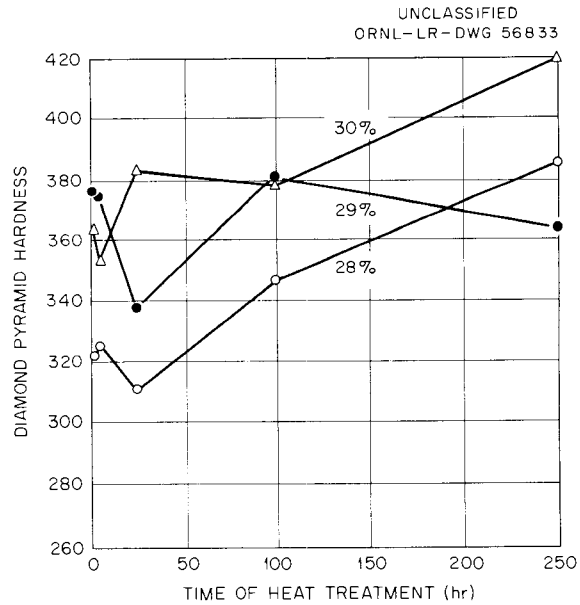

Fig. 22. Effect of Composition and Time of Heat Treatment on Hardness of 28, 29, and 30 wt % Molybdenum Alloys Aged at 800°C. As-quenched hardness given in Fig. 19.

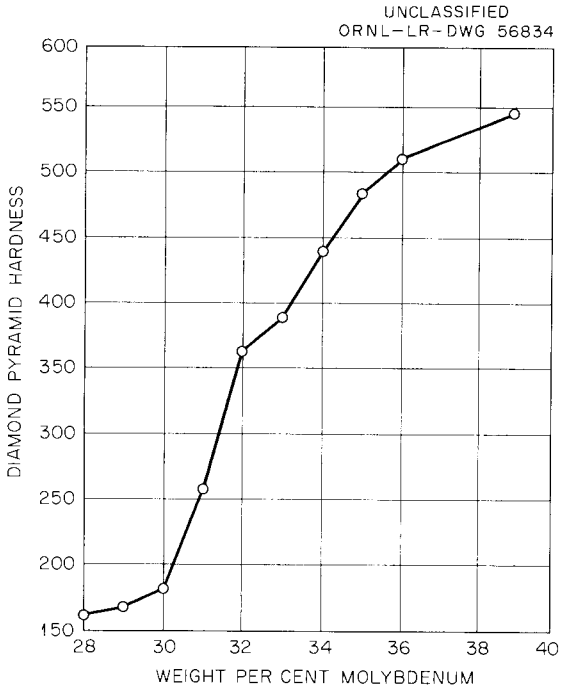

Fig. 23. Effect of Composition on Hardness of Alloys Heat Treated at 872°C for 150 hr.

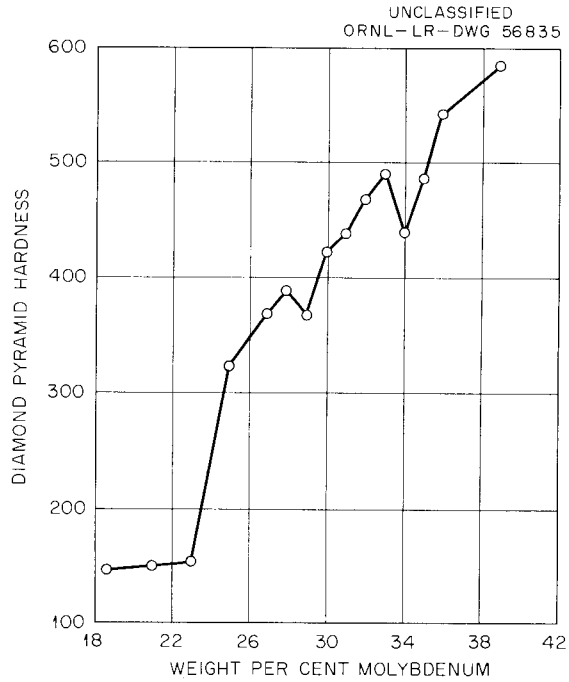

Fig. 24. Effect of Composition on Hardness of Alloys Heat Treated at 800°C for 250 hr.

DISCUSSION OF RESULTS

This research has resulted in a re-evaluation of a portion of the nickel-rich end of the nickel-molybdenum phase diagram. The proposed diagram is presented in Fig. 11. The present discussion is concerned with the correlation of the microstructural, x-ray, and hardness data which were used to establish the diagram. As previously mentioned, only a portion of the total data taken during the course of the research will be considered. The discussion is presented in sections, each considering evidence in support of the proposed boundaries of the single- or two-phase regions within the diagram. Inconsistencies and problems arising during the investigation are discussed where pertinent.

The α Phase

The solid solution range of molybdenum in nickel was substantiated as varying quite widely with temperature. At 600°C a maximum solubility of approximately 19 wt % molybdenum was determined, while at 1250°C a solubility of approximately 37% was observed. Other points within this

range included solubilities of 32% at 910°C, the γ decomposition temperature, and 29% at 868°C, the β decomposition temperature.

A lattice expansion of about 0.0033 A per weight per cent molybdenum was found to be useful in establishing several points on the α-α plus β phase boundary. Unfortunately, above 850°C uncertainties in the lattice parameters limited this procedure for establishing phase boundaries, and, therefore, estimates based on the results of metallographic examinations became more reliable. Films yielding uncertainties in the α parameters showed the appearance of a new set of weak lines inconsistent with the diffraction lines of any established phase in the system. Considerable, but unsuccessful, effort was made to establish the identity of these weak diffraction lines.

At first it was thought that these weak lines were the result of one or more impurities entering the sample during the filing process and during heat treatment. In fact, spectrographic analysis showed sufficient quantities of silicon and iron to justify such a conclusion. To investigate this possibility a new series of specimens was prepared and heat treated in a manner minimizing silicon and iron contamination. These specimens, prepared from the sintered compacts in the form of small cylindrical rods, were sealed in evacuated Vycor capsules, along with filings of the same alloy composition. The filings served to prevent the specimen from making contact with the capsule wall and also to absorb the major part of any volatile material which might have been in the capsule. The specimens were then heat treated at various temperatures, etched to remove any surface effects, and analyzed by x-ray diffraction. These unidentified weak lines were still present with very little change in intensity, although parameter inconsistencies were reduced somewhat.

To investigate the possibility of complex oxides, nitrides, or hydrides, various pressures of air and hydrogen were imposed upon filings during heat treatment. These, too, had very little effect, if any, on the intensity of the weak lines.

The interplanar spacings of the planes producing these weak lines were compared with those listed in the ASTM files for all oxides, nitrides, and carbides of nickel and molybdenum. These, also, could not account for the unidentified lines.

At this point, being unable to establish any clue to their source, it was concluded that these weak unidentified lines must be contributed by a metastable phase existing within the system. A superlattice is a possibility but appears rather improbable at this state of the investigation. A summary of the conditions under which the weak diffraction lines were seen to exist is as follows: temperature range – above 800°C; composition range – 26 to 36 wt % molybdenum; quenching rates – any quenching rate rapid enough to prevent excessive blurring of the back reflection diffraction region.

Table B-3 in Appendix B contains the observed intensities and θ values for these lines. The observations were made on a Debye pattern of a 34 wt % molybdenum solid specimen which had been heat treated at 1000°C for 72 hr.

The β Phase – Ni_4Mo

The major disagreement in the constitutional diagram data published on the nickel-molybdenum alloy system to date lies in the interpretation of alloys containing about 20 at. % molybdenum. Early work on alloys in this composition range by Grube and Schlect (1), publishers of the first nickel-molybdenum phase diagram, identified this region as containing a single phase, β, corresponding to the compound Ni_4Mo and having a face-centered tetragonal unit cell with a c/a ratio of approximately 0.98. They also reported evidence of a superstructure existing for alloys lying to the nickel-rich side of the Ni_4Mo composition. From their work in this region, which was based primarily on x-ray studies, it was not possible to establish the details of the ordering reaction.

The more recent phase diagram established by Ellinger (3) interprets the region on the nickel-rich side of Ni_4Mo as a two-phase region containing the nickel-rich solid solution as well as β, the β being the result of a solid solution precipitation phenomenon. His work was based primarily on microscopic examinations and hardness data.

As will be discussed shortly, x-ray data obtained in this investigation have established that the structure of the β phase can be derived from the α phase by the equivalence of ordering of the molybdenum atoms

and allowing a slight shift in interplanar distances. This derivation leads to a β unit cell identical with the one proposed by Harker (4).

For an α phase of the Ni_4Mo composition existing at high temperature, a mechanism of conversion to β of exactly Ni_4Mo composition must be considered. The mechanism does not require bulk diffusion of either species. However, if the composition is not stoichiometric, it becomes necessary to propose either that a nonstoichiometric ordered phase will form, or that, at some stage, bulk diffusion of the species will occur, with the formation of two-phase structures.

In the nickel-molybdenum system it is possible to study the transformation of α to structures containing both greater and smaller amounts of molybdenum than required for Ni_4Mo. For compositions extending from the α solubility limit to Ni_4Mo, metallographic studies made during this investigation have shown a precipitation-type phenomenon. The precipitating phase is observed to grow from the α matrix in a variety of forms, ranging from very fine precipitates to highly developed Widmanstätten or lamellar structures. These observations confirm those reported by Ellinger (3).

Since a Widmanstätten structure is observed also for the exact Ni_4Mo composition, at least for this alloy there is no way to rationalize that a second phase exists at equilibrium. Of course during the formation of β from α, two-phase structures are expected. However, the Widmanstätten structure persists after all α, detectable by x-ray methods, is gone.

Considering the results of both x-ray and metallographic studies, it was concluded that β may be considered as an ordering of the α phase. Beta nucleates and grows with crystallographic relationship to the matrix α, undoubtedly with coherency existing between ordered plates of β and the disordered α matrix. Strain at this stage of transformation could account for the observed etching effects. With further growth of a β plate, both laterally and in thickness, β plates will finally impinge. If consideration is given to the particularly simple case of platelets of β having randomly nucleated on different planes of a given set of parallel matrix planes, it is evident that there will be a mismatch in the order as successive platelets of β finally meet when the

last α between them transforms. These disorder boundaries could give rise to etching effects in "pure" β. Typical structures of "pure" β are shown in Figs. 12-14 and 12-20.

Other alloy systems which exhibit x-ray diffraction evidence of order-disorder states existing together in equilibrium are the cobalt-platinum (8), the nickel-platinum (9), and the gold-copper (10) systems.

Evidence of an Ordered Structure

Alloys of the theoretical β composition, 29.02 wt % molybdenum, quenched from temperatures above 868°C, produce Debye-Scherrer x-ray patterns characteristic of the nickel-rich face-centered cubic solid solution. X-ray patterns of this alloy heat treated below this temperature show a splitting of these lines into two or three components, with the exception of the (111) and (222) planes. In addition to this line splitting, numerous other faint lines resembling those characteristic of an ordering reaction appear upon further aging at these temperatures. Neglecting these faint lines, these patterns can readily be indexed as the face-centered tetragonal structure reported in earlier literature. However, as Harker (4) pointed out, it is impossible to account for these new "superstructure" lines on the basis of this face-centered tetragonal cell.

Derivation of Ordered Cell

Approaching the problem from an atomistic point of view, that is, arranging the molybdenum atoms on the α lattice to form an ordered structure with an atom ratio of four nickel to one molybdenum, several superlattices are readily deduced. Of these, only one will be discussed because it is the simplest and places the molybdenum atoms at a maximum distance from each surrounding molybdenum atom, which would normally be expected in an ordered structure.

The following scheme was used: molybdenum atoms are placed in every fifth position in a [110] direction on a (100) plane. Molybdenum atoms on successive [110] rows of atoms are arranged, in a systematic manner, so as to be at the greatest distance from the molybdenum atoms on the previous [110] row, as shown by Fig. 25.

If a second (100) plane of atoms, arranged exactly as the first, were placed so that the molybdenum atoms contained by it fall directly above the positions marked by the x's, and then a third similar plane of atoms were superimposed directly above the first, an ordered lattice is seen to develop. This ordered lattice would then be described in terms of a new unit cell containing eight nickel and two molybdenum atoms. Its basic structure is that of a body-centered tetragonal cell and could be treated as five interpenetrating lattices of the body-centered tetragonal type — one of pure molybdenum and four of pure nickel.

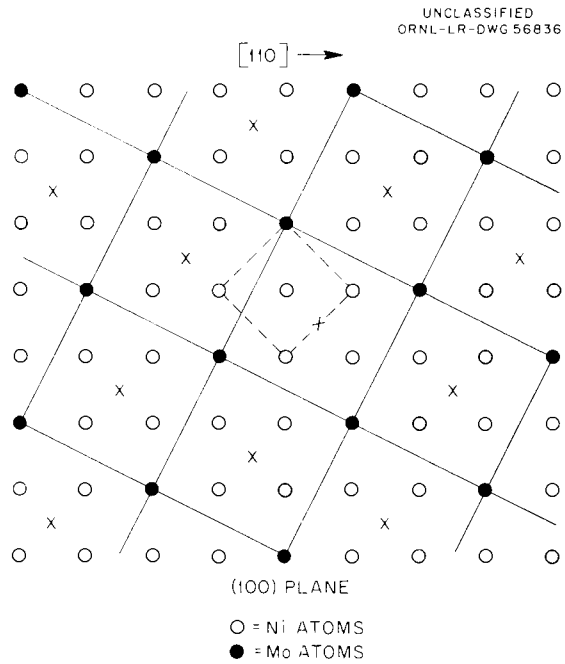

Fig. 25. Schematic Drawing of Ordering Process. Dotted lines outline face-centered cubic cell.

Miller indices were then determined for several diffracting planes within this tetragonal cell by relating them to their equivalent face-centered cubic diffracting planes (see Appendix A). Using these prescribed indices, it was then found possible to further assign indices to all the β lines observed on the Debye patterns. The intensities of these lines were then calculated, using Lorentz, polarization, multiplicity, and structure factors. The results of these calculations appear in Table 1, along with the observed and calculated intensities and θ values. Since the observed and calculated intensities are in good agreement, the structure is assumed to be correct. Parameters determined for this cell were: $a_0 = 5.727$ A, $c_0 = 3.566$ A, and $c/a = 0.623$. These parameters are in very good agreement with those determined by Harker (4) for a 27.3 wt % molybdenum alloy. The intensity calculations listed here are not in good agreement with those determined by Harker. These differences are not understood, although similar equations were used. However, agreement between observed and calculated intensities made in this

Table 1. Calculated and Observed Intensities for an X-Ray Powder Diffraction Pattern of a 29 wt % Molybdenum Alloy Heat Treated at 825°C for 46 hr[a]

$hk\ell$[b]	θ Observed	I Calculated[c]	I Observed[d]
110	11.11	1.57	m wk
101	14.90	1.33	m wk
200	15.76	0.59	wk
211	21.85	44.18	v st
220	22.48	0.22	wk
310	25.33	14.00	st
002	25.78	6.47	m st
301	27.41	0.28	wk
112	28.35	0.22	wk
202	30.73	0.18	wk
321	32.19	0.30	wk
400	33.06	0.07	v wk
330	34.89	0.05	v wk
222	35.27	0.11	wk
411	36.69	1.00	m wk
420	37.11	4.14	m st
312	37.49	8.00	st
103	41.57	0.07	v wk
510	43.41	0.06	v wk
402	43.76	0.06	v wk
501, 431	45.00	11.07	st
213, 332	45.67	5.19	m st
422	47.85	4.82	m st
422	48.05	2.41	m
521, 440	49.19	0.14	wk
303	49.75	0.06	v wk
530	51.79	0.06	v wk
600, 323, 512	54.15	0.26	m wk
611	57.89	0.12	wk
620 α_1	58.36	2.32	m wk
620 α_2, 413	58.60	1.28	m wk
004 α_1	59.81	1.20	m wk
004 α_2	60.10	0.60	wk
442	61.08	0.06	v wk
114	62.30	0.06	v wk
541	62.65	0.13	wk
532 α_1	63.56	0.14	wk
532 α_2	63.93	0.07	v wk
204 α_1	64.88	0.08	v wk
204 α_2	65.19	0.04	v wk
602 α_1	66.35	0.08	v wk
602 α_2	66.66	0.04	v wk
631 α_1	68.15	6.17	m st

Table 1 (continued)

$hk\ell$[b]	θ Observed	I Calculated[c]	I Observed[d]
631 α_2	68.50	3.09	m
503 α_1, 433 α_1	69.10	12.75	st
503 α_2, 433 α_2	69.47	6.37	m st
224 α_1	70.76	0.09	v wk
224 α_2	71.20	0.05	v wk
710 α_1, 550 α_1	72.05	10.94	m st
710 α_2, 550 α_2, 622 α_1	72.59	13.07	st
622 α_2	73.05	7.60	m
314 α_1	74.40	8.46	st
314 α_2	74.94	4.23	m
640 α_1	75.87	0.13	v wk
640 α_2, 523 α_1	76.42	0.33	wk
523 α_2	77.02	0.14	v wk

[a]Nickel-filtered copper Kα radiation was used.

[b]Individual K components where resolved are indicated by the subscripts.

[c]In general, the intensities of ($hk\ell$) and ($kh\ell$) are not the same, but since they both diffract at the same angle, their intensities were added to give the calculated intensity listed opposite ($hk\ell$) in the table.

[d]v st = very strong m = medium m wk = medium weak
st = strong wk = weak
m st = medium strong v wk = very weak

investigation is better than those reported by Harker (4). The following discussions regarding β are based on this cell determination.

Discussion of Structure

The atomic arrangement of the Ni_4Mo unit cell is very close to cubic close packing, with each atom having 12 nearest neighbors. Each molybdenum atom has 12 nearest neighbors all of which are nickel, and each nickel atom has three molybdenum and nine nickel atoms as nearest neighbors.

Perhaps the most important and interesting factor governing the unusual physical properties that are observed as the β ordering process occurs is that there are 30 possible ways for β to nucleate from a single α lattice. Referring to Fig. 25, each one of the first five atoms in the

[110] row could serve equally well as the origin of the structure. Secondly, the tetragonal a axis can be inclined either positively or negatively to this [110] direction. Finally, this (100) plane can be any one of the three cube planes. Thus, $5 \times 2 \times 3 = 30$. Of these, however, only six will produce different orientations of β, each having five starting positions.

It is reasonable to assume that local distortions of the original cubic structure, such as would be produced by forming complicated arrays of Ni_4Mo crystals within the cubic lattice, would make slip very difficult and explain the problems encountered in the cold working of alloys of this composition. The increase in hardness which accompanies this ordering reaction can also be explained on this basis.

β Plus α

X-ray patterns of β in equilibrium with α usually show two triplet formations in the regions of the original α (200) and (311) lines. Two lines of each triplet develop with the β tetragonal cell, the third being the original α line. These can be seen from the photograph of Fig. 14-1. Observed θ values and intensities for this pattern are given in Table B-4 in Appendix B.

When parameters of both cells are compatible, only doublets are formed, the α line being superimposed with one of the β lines. In these cases, critical line intensity comparisons must be made in order to distinguish a mixture of β and α from pure β.

Metallographically, β is seen to form in α as both finely dispersed particles and in platelets, producing sharp striations within the original α grains. Near the α phase boundary this fine dispersion of β in α is the most predominant, as seen in Figs. 12-18, 12-25, and 12-26. At longer periods of aging, these β formations tend to coarsen somewhat (Figs. 12-25 to 12-27), but do so at a very slow rate.

In alloys near the β composition, the striations which develop within the solid solution grains are the primary identification features of β (Figs. 12-20 and 12-28). This striated appearance develops within a few hours and remains essentially unchanged after several hundred hours of heat treatment. Figure 12-19 shows β as both finely dispersed and

striated, as was consistent throughout specimens examined within this intermediate composition range.

In all the specimens exhibiting sharp striations only three different directions of plate traces were observed, indicating a $(100)_\alpha$ habit plane for the formation of β in α. Preferential growth of β along either the tetragonal a or c axis would produce β as plates exhibiting a $(100)_\alpha$ habit plane, as both are parallel to (100) planes of the parent cubic lattice. It is reasonable to assume, however, that preferential growth would occur along a direction of greatest match between the two lattices. Shrinkage factors determined for the ordering reaction were approximately 0.5 and 1.0% in the tetragonal a and c axes, respectively. Thus, one could conclude that the observed preferential growth is along any one of the three {100} planes of the matrix, but in every case the (001) planes of β are parallel to the matrix cube plane.

All specimens heat treated within this α plus β region, with the exception of the 18.7 wt % molybdenum alloy, responded readily to heat treatment, producing rapid hardness increases in a few tenths of an hour, as seen by Figs. 20, 21, and 22. Continued aging periods beyond 5 hr, in most cases, resulted in a rapid hardness decrease. This is in turn followed by another hardness increase, but of a more gradual nature. These exhibited double aging peaks are not fully understood.

Reviewing previously discussed x-ray observations of similar aging periods, it was observed that short-time treatments produced Debye patterns showing the formation of a face-centered tetragonal cell. Continued aging times produced the weak superlattice lines of the fully ordered body-centered tetragonal cell. A reasonable correlation between x-ray and hardness data could be interpreted as follows: In very short aging times a partially ordered structure, β', is formed coherently in the α lattice, producing a rapid hardness increase. As coherency is lost by the formation of the fully ordered cell, β, hardness decreases. Continued formation and growth of β could then reasonably account for the second aging peak of the hardness curves. Schematically this could be shown as follows:

$$\alpha_{fcc} \rightarrow \beta'_{fct} \rightarrow \beta_{bct} \ .$$

The γ Phase — Ni_3Mo

Alloys of the theoretical γ composition heat treated above 910°C produce x-ray diffraction patterns showing primarily α plus a small amount of δ. Slightly below this temperature δ is seen to disappear, with a large amount of γ appearing, but still some α present. As the temperature is decreased, the relative amount of α decreases. These trends can be seen in Figs. 15-1 through 15-3.

The phase Ni_3Mo has been reported to have a hexagonal close-packed lattice (2), with a = 2.545 A and c/a = 1.65. The lines of the x-ray photograms obtained in this investigation were analyzed on the basis of this prescribed cell, with the results shown in Table 2. As can readily be seen, this hexagonal close-packed cell does not account for the three doublets observed in the principal lines characterizing the γ phase as

Table 2. Comparison of Calculated and Observed Diffraction Lines for Ni_3Mo*

θ Observed	θ Calculated	$hk\ell$ for Calculated Values
20.40 20.63	20.35	100
21.58	21.65	002
23.18 23.40	23.18	101
30.47	30.47	102
37.27 37.62	37.00	110
40.65	40.80	103
44.00 44.87	44.01 44.93	200 112
46.40	46.00	201

*Comparison of gamma lines observed with those calculated for a hexagonal close-packed cell with a = 2.545 A and c/a = 1.65. Powder specimen was taken from a 32.01% molybdenum alloy and heat treated at 872°C for 64 hr.

Only principal lines observed for the γ phase. For additional lines see Table B-6 in Appendix B.

Nickel-filtered copper Kα radiation was used.

well as numerous faint lines which are not given in this table. These faint lines resemble those characteristic of a superstructure, similar to those encountered in the β phase. Also these doublets have the same ratio of their sine-squared values, 0.98, as was found in the β phase. These conditions suggest that a superlattice exists in this region, and, if so, it must be very close to the described hexagonal close-packed structure.

An attempt was made to determine the structure of Ni_3Mo on this basis, but it was unsuccessful because a satisfactory agreement between observed and calculated intensities could not be reached.

Figure 12-12 shows a typical γ structure as recrystallized from large-grained α. The dark needlelike formations and the precipitation outlining some of the original α grain boundaries are residual δ particles resulting from previous homogenizations.

β Plus γ

Figures 12-29 through 12-32 show progressively the formation of β plus γ from large-grained α. In the 30 and 31% specimens the transformation is occurring by a process of nucleation and growth principally from the grain boundaries and resulting in a lamellar structure consisting of β and γ. The 32% specimen is entirely consumed by this β-γ structure. Still closer to the γ composition, as in the 33% specimen, regions unconsumed by this precipitate occur again. At 34% (see Fig. 12-23), the structure becomes predominantly single-phase γ.

Hardness measurements of the 30 and 31% specimens revealed that the hardness of the unconsumed regions is almost identical to that of the β-γ precipitate. This, and the fact that the hardness is reached in a very short time, suggests that formation of a metastable precipitate in α of a metastable β of the higher molybdenum composition precedes that of the lamellar growth and is absorbed by this growing interface, although it has not been observed metallographically in this investigation. Stoffel (6), however, did observe a precipitate to form within the original α grains of 30% alloys, followed by nucleation and growth of this lamellar structure. His work did not establish the structure or mechanism of this precipitation.

Spectrometer traces of 30% alloys investigated in this experiment produced diffraction peaks at positions equivalent to those of the β (110) and (002) lines after aging periods of only 1 hr. As nucleation and growth of the β-γ structure become microscopically resolvable, more prominent β peaks plus those characteristic of γ become visible. As growth continues, these β and γ peaks become more and more prominent. These conditions indicate that a metastable precipitation of β precedes the formation of the β-γ structure. However, it is felt that sufficient evidence has not been obtained to justify a definite conclusion at this time.

α Plus γ

In the α plus γ region, γ normally precipitated from α as plates, forming banded grains composed of alternate layers of α and γ. Typical structures showing these banded grains are seen in Figs. 12-6 and 12-11. Near the α-γ phase boundary, γ has a tendency to form as a precipitation outlining the original α grains (Fig. 12-5). Also, the small oval-shaped particles sparsely scattered throughout the α matrix are γ formations. A typical set of measurements showing hardness trends across this region is shown in Fig. 23.

The δ Phase — NiMo

Although the major purpose of this investigation was to either verify or correct the nickel-rich portion of the existing constitutional diagram, an alloy of the theoretical δ composition, 62.01 wt % molybdenum, was prepared. This alloy was developed by the aforementioned powder metallurgy techniques and was intended solely for identification purposes when δ coexists with α or γ. X-ray patterns of this specimen showed numerous diffraction lines, indicating a complex structure, even more complex than that of β or γ. A structure determination for this phase was not attempted. Table B-7 in Appendix B contains the observed θ values and intensities for this alloy.

Figures 12-2, 12-3, and 12-4 show progressively the development of δ in an α matrix. Near the α-δ phase boundary, δ is seen to develop primarily as a precipitation outlining the original α grains. Figure

12-3 shows a more uniform precipitation of δ in α at a slightly higher molybdenum content. At a still higher molybdenum concentration the formation of the α plus δ eutectic structure is clearly shown (Fig. 12-4).

CONCLUSIONS

This investigation has led to a re-evaluation of the nickel-rich portion of the nickel-molybdenum diagram. The results of this investigation permit the following conclusions:

1. The β peritectoid temperature has been established at 868°C.
2. The γ peritectoid temperature has been established at 910°C.
3. Necessary changes in phase boundaries consistent with these decomposition temperature establishments have been made.
4. The β phase has been confirmed to have a body-centered tetragonal unit cell, belonging to the C_{4h}^{5}–I4/m space group as reported by Harker (4).
5. The γ phase does not possess a simple close-packed hexagonal unit cell as reported in earlier literature. Its structure, not established by the results of this investigation, is complicated by numerous faint diffraction lines characteristic of a superstructure, as well as several distinct diffraction lines not accounted for on the basis of the previously reported unit cell.
6. X-ray data and hardness measurements have indicated that several of the final equilibrium structures are preceded by the formation of a metastable precipitate. The mechanism of this formation has not been established.

LIST OF REFERENCES

(1) G. Grube and H. Schlect, "Elektrische Leitfähigkeit und Zustandsdiagramm bei binären Legierrungen Das System Nickel-Molybdän," Z. Elektrochem. 44, 413 (1938).

(2) G. Grube and O. Winkler, "Magnetische Suszeptibilität und Zustandsdiagramm von binären Legierungen Das System Nickel-Molybdän," Z. Elektrochem. 44, 423 (1938).

(3) F. H. Ellinger, "The Nickel-Molybdenum System," Trans. Am. Soc. Metals 30, 607 (1942).

(4) D. Harker, "The Crystal Structure of Ni_4Mo," J. Chem. Phys. 12, 315 (1944).

(5) D. S. Bloom and N. J. Grant, "An Investigation of the Systems Formed by Chromium, Molybdenum, and Nickel," Trans. AIME 200, 261 (1954).

(6) D. W. Stoffel, "A Metallographic and X-Ray Study of Nickel Alloys of 20–30 Percent Molybdenum," M.S. Thesis, University of Tennessee, 1955.

(7) M. J. Buerger, X-Ray Crystallography, p 401, Wiley, New York, 1942.

(8) J. B. Newkirk et al., "Ordering Reaction in Cobalt-Platinum Alloys," Trans. AIME 188, 1249 (1950).

(9) U. Esch and A. Schneider, "Das System Nickel-Platin," Z. Elektrochem. 50, 268 (1944).

(10) J. L. Haughton and R. J. M. Payne, "Transformations in the Copper-Gold Alloys," J. Inst. Metals 46, 457 (1931).

Appendix A

CORRELATION OF TETRAGONAL AND CUBIC INDICES

Referring to Fig. A-1, the relationship between equivalent diffracting planes in the body-centered tetragonal cell and the original face-centered cubic cell can readily be calculated as follows:

$$\tan\theta = \frac{a/\sqrt{2}}{2a/\sqrt{2}} = \frac{1}{2}\,, \qquad (1)$$

and

$$\sin\theta = \sin\left(\tan^{-1}\frac{1}{2}\right) = \frac{a/\sqrt{2}}{a'}\,. \qquad (2)$$

Hence,

$$a' = 1.581a\,, \qquad (3)$$

where a' is the lattice parameter of the tetragonal cell and a is the parameter of the original cubic lattice.

Since the cell directions in the Z direction are identical,

$$c' = a\,. \qquad (4)$$

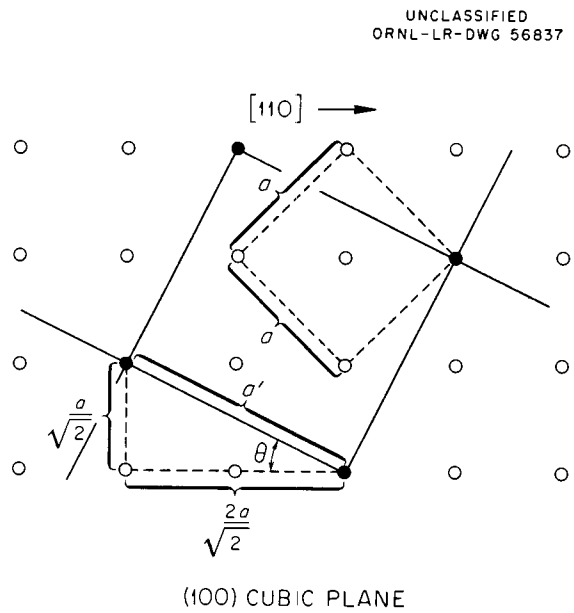

Fig. A-1. Schematic Drawing of Ordering Reaction.

Thus, the volume V' of this new cell is seen to be 2.5 times the volume of the original cubic cell:

$$V' = a'^2c' = 2.5a^3\,. \qquad (5)$$

The angles of the rays diffracted from the cubic cell would be governed by the Bragg equation of the form

$$\sin^2\theta = \frac{\lambda}{4a^2}\left(h^2 + k^2 + \ell^2\right)\,, \qquad (6)$$

while the rays diffracted by the tetragonal cell would be governed by an equation of the form

$$\sin^2\theta = \frac{\lambda}{4}\left(\frac{h'^2 + k'^2}{a'^2} + \frac{\ell'^2}{c'^2}\right)\,. \qquad (7)$$

Since all lattice sites have been conserved in deriving this new cell from the α lattice, the diffracting angles of identical planes would be the same; thus,

$$\frac{h^2 + k^2 + \ell^2}{a^2} = \frac{h'^2 + k'^2}{a'^2} + \frac{\ell'^2}{c'^2} , \tag{8}$$

and, substituting for a' and c' in terms of a,

$$h^2 + k^2 + \ell^2 = \frac{h'^2 + k'^2}{2.5} + \ell'^2 . \tag{9}$$

This expression is the relationship between the indices of identical planes of the two cells. We can even go further and say that the ℓ terms of the two cells must be equivalent; thus, this expression becomes

$$2.5 \times (h^2 + k^2) = h'^2 + k'^2 . \tag{10}$$

From this expression it is readily seen that the original face-centered cubic indices – (111), (200), (220), etc. – must now become the (211), (310), (420), etc., of the ordered body-centered tetragonal cell.

Appendix B

HARDNESS DATA AND ANALYSIS OF DEBYE-SCHERRER X-RAY FILMS

Table B-1. a_0 Values for α Solid-Solution Alloys

Composition (wt % molybdenum)	a_0 (A)
18.00	3.5724
20.00	3.5793
22.01	3.5853
24.02	3.5917
26.02	3.5970
27.98	3.6042
29.00	3.6080
30.00	3.6105
32.01	3.6180

Table B-2. Hardness Data

Composition (wt % molybdenum)	Aging Temperature (°C)	Aging Time (hr)	Diamond Pyramid Hardness
18.7	1000	17	119.4
21	1000	17	136.8
23	1000	17	140.7
25	1000	17	150.0
27	1000	17	155.5
28	1000	17	160.0
29	1000	17	160.0
30	1000	17	159.2
31	1000	17	167
32	1000	17	173
33	1000	17	180
34	1000	17	182
35	1000	17	297
36	1000	17	283
39	1000	17	339
28	865	1	348
28	865	5	351
28	865	25	322
28	865	100	378
28	865	150	346
28	825	1	321
28	825	5	347
28	825	25	340
28	825	100	347
28	825	150	377
28	800	1	323
28	800	5	326
28	800	25	312
28	800	100	347
28	800	250	384
29	865	1	388
29	865	5	375
29	865	25	383
29	865	100	375
29	865	150	378
29	825	1	360
29	825	5	374
29	825	25	345
29	825	100	342
29	825	150	369
29	800	1	364
29	800	5	354
29	800	25	384
29	800	100	378
29	800	250	363

Table B-2 (continued)

Composition (wt % molybdenum)	Aging Temperature (°C)	Aging Time (hr)	Diamond Pyramid Hardness
30	865	1	353
30	865	5	359
30	865	25	354
30	865	100	355
30	865	150	334
30	825	1	377
30	825	5	400
30	825	25	367
30	825	100	391
30	825	150	436
30	800	1	376
30	800	5	375
30	800	25	339
30	800	100	380
30	800	250	420
28	872	150	161
29	872	150	167
30	872	150	182
31	872	150	257/185
32	872	150	363
33	872	150	387
34	872	150	437
35	872	150	482
36	872	150	509
39	872	150	544
18.7	800	250	148
21	800	250	150
23	800	250	153
25	800	250	323
27	800	250	363
28	800	250	384
29	800	250	363
30	800	250	420
31	800	250	436
32	800	250	464
33	800	250	488
34	800	250	437
35	800	250	484
36	800	250	539
39	800	250	583

Table B-3. Analysis of a Debye-Scherrer X-Ray Film of a 34% Molybdenum Alloy Heat Treated at 1000°C for 48 hr[a]

θ[b]	I Observed[c]	$hk\ell - \alpha$[b]	θ[b]	I Observed[c]	$hk\ell - \alpha$[b]
16.54	wk		58.12 α_1	wk	
18.06	wk		58.39 α_2	m wk	400
21.64	m wk		59.10 α_1	wk	
21.71	st	111	59.39 α_2	v wk	
23.70	m wk		60.73 α_1	wk	
25.29	m st	200	60.99 α_2	wk	
28.07	v wk		66.51 α_1	v wk	
30.44	wk		67.70 α_1	wk	
32.99	wk		68.00 α_2, α_1	m	331 α_1
35.47	wk		68.36 α_2	m	331 α_2
37.04	m st	220	71.15 α_1	wk	
37.86	wk		71.60 α_2	wk	
40.23	v wk		72.02 α_1	m	420 α_1
40.51	v wk		72.48 α_2	m	420 α_2
45.01	m	311	73.65 α_1	wk	
46.08	wk		74.12 α_2	v wk	
47.13	wk		75.27 α_1	wk	
47.62	m wk	220	75.86 α_2	v wk	
51.88	v wk		78.50 α_1	wk	
54.15 α_1	v wk		79.27 α_2	v wk	
55.65 α_1	wk		80.92 α_1	v wk	
55.86 α_2	v wk		81.86 α_2	v wk	

[a]Nickel-filtered copper radiation was used.

[b]Individual k components where resolved are indicated by subscripts following the θ values.

[c] st = strong; m = medium; wk = weak; m st = medium strong; m wk = medium weak; v wk = very weak

Table B-4. Analysis of a Debye-Scherrer X-Ray Film of a 29% Molybdenum Alloy Heat Treated at 830°C for 142 hr*

θ	I Observed**	$hk\ell - \beta$	$hk\ell - \alpha$
11.06	wk	110	
14.87	m wk	101	
15.69	wk	200	
21.89	v st	211	111
25.30	m st	310	
25.51	m st		200
25.72	m	002	
37.06	m	420	
37.46	st	312	
45.07	m st	501, 431	
45.44	m st		311
45.74	m	213, 332	
47.96	m	422 α_1	
68.32	m	631 α_1	
68.53	m wk	631 α_2	
69.11	st	503 α_1, 433 α_1	
69.53	m st	503 α_2, 433 α_2	
72.03	m wk	710 α_1, 550 α_2	
72.57	m	710 α_2, 550 α_2, 622 α_1	
73.08	v wk	622 α_2	
74.41	m wk	314 α_1	
74.98	wk	314 α_2	

*Nickel-filtered copper radiation was used.

**v st = very strong
st = strong
m st = medium strong
m = medium
m wk = medium weak
wk = weak
v wk = very weak

Table B-5. Analysis of a Debye-Scherrer X-Ray Film of a 30% Molybdenum Alloy Heat Treated at 846°C for 90 hr[a,b]

θ	I Observed[c]	$hk\ell - \beta$
11.09	m wk	110
14.87	m wk	101
15.76	wk	200
21.86	v st	211
25.30	st	310
25.76	m st	002
27.41	v wk	301
28.25	v wk	112
30.74	v wk	202
32.24	wk	321
36.59	v wk	411
37.08	m	420
37.45	m st	312
45.04	st	501, 431
45.70	m st	213, 332
47.89	m st	422
58.35	m wk	620 α_1
58.62	wk	620 α_2, 413
59.82	wk	004 α_1
68.11	m	631 α_1
68.48	m wk	631 α_2
69.06	st	503 α_1, 433 α_1
69.44	m st	503 α_2, 433 α_2
72.00	m	710 α_1, 550 α_1
72.53	m st	710 α_2, 550 α_2, 622 α_1
73.04	m	622 α_2
74.38	m st	314 α_1
74.93	m	314 α_2
76.41	wk	523 α_1
76.88	v wk	523 α_2

[a]Nickel-filtered copper radiation was used.

[b]A very faint trace of gamma was observable but not indexable on this film.

[c]v st = very strong; st = strong; m st = medium strong; m = medium; m wk = medium weak; wk = weak; v wk = very weak

Table B-6. Analysis of a Debye-Scherrer X-Ray Film of a 35.27% Molybdenum Alloy Heat Treated at 846°C for 90 hr*

θ	I Observed**
9.37	v wk
10.14	v wk
13.44	wk
13.90	wk
14.72	wk
16.50	v wk
17.21	wk
17.77	v wk
20.38	m wk
20.62	m
21.58	m st
23.17	m st
23.42	st
25.71	v wk
28.55	v wk
29.89	v wk
30.53	m
31.92	v wk
34.95	v wk
37.11	m
37.60	m wk
40.64	m
42.99	v wk
43.93	wk
44.88	m
45.36	m wk
45.82	m wk
46.50	m
47.13	m wk

*Nickel-filtered copper radiation was used.

** st = strong
m st = medium strong
m = medium
m wk = medium weak
wk = weak
v wk = very weak

Table B-7. Analysis of a Debye-Scherrer X-Ray Film of a 62% Molybdenum Alloy Heat Treated at 851°C for 146 hr*

θ	I Observed**
16.81	wk
18.67	m wk
20.53	m st
21.12	m wk
21.72	m st
22.05	st
22.32	m wk
22.91	m
23.62	m wk
24.67	wk
25.03	m wk
25.36	wk
26.10	v wk
29.23	v wk
29.89	v wk
31.56	v wk
32.17	v wk
33.39	v wk
33.90	wk
34.66	wk
35.15	wk
37.17	m wk
37.96	m wk
38.51	m wk
41.04	wk

*Nickel-filtered copper radiation was used.

** st = strong
m st = medium strong
m = medium
m wk = medium weak
wk = weak
v wk = very weak

ORNL-3078
UC-25 – Metals, Ceramics, and Materials
TID-4500 (16th ed.)

INTERNAL DISTRIBUTION

1. C. E. Center
2. Biology Library
3. Health Physics Library
4. Metallurgy Library
5-6. Central Research Library
7. ORNL-Y-12 Technical Library
8. Reactor Division Library
9-17. Laboratory Records Department
18. Laboratory Records, RC
19. J. P. Murray (K-25)
20. G. M. Adamson, Jr.
21. J. O. Betterton, Jr.
22. D. S. Billington
23. A. L. Boch
24. E. G. Bohlmann
25. B. S. Borie
26. C. J. Borkowski
27. D. T. Bourgette
28. G. E. Boyd
29. E. J. Breeding
30. R. B. Briggs
31. J. V. Cathcart
32. R. A. Charpie
33. G. W. Clark
34. R. E. Clausing
35. R. S. Cockreham
36. Esther Cohn
37. F. L. Culler
38. J. E. Cunningham
39. J. H. DeVan
40. D. A. Douglas, Jr.
41. A. P. Fraas
42. J. H. Frye, Jr.
43. W. R. Grimes
44. J. P. Hammond
45. W. O. Harms
46. C. S. Harrill
47-51. M. R. Hill
52. E. E. Hoffman
53. A. Hollaneder
54. A. S. Householder
55. H. Inouye
56. R. G. Jordan (Y-12)
57. C. P. Keim
58. M. T. Kelley
59. J. A. Lane
60. S. C. Lind
61. R. S. Livingston
62. T. S. Lundy
63. H. G. MacPherson
64. W. D. Manly
65. R. W. McClung
66. D. L. McElroy
67. C. J. McHargue
68. A. J. Miller
69. E. C. Miller
70. K. Z. Morgan
71. M. L. Nelson
72. A. R. Olsen
73. P. Patriarca
74. D. Phillips
75. M. L. Picklesimer
76. P. M. Reyling
77. H. W. Savage
78. J. L. Scott
79. H. E. Seagren
80. E. D. Shipley
81. M. J. Skinner
82. C. O. Smith
83. G. P. Smith, Jr.
84. A. H. Snell
85-104. E. E. Stansbury (consultant)
105. J. A. Swartout
106. A. Taboada
107. E. H. Taylor
108. W. C. Thurber
109. A. M. Weinberg
110. G. C. Williams
111. C. E. Winters
112. H. L. Yakel, Jr.
113. J. L. Gregg (consultant)
114. C. S. Smith (consultant)
115. R. Smoluchowski (consultant)
116. H. A. Wilhelm (consultant)
117. J. H. Koenig (consultant)

EXTERNAL DISTRIBUTION

118. Division of Research and Development, AEC, ORO
119. F. N. Rhines, University of Florida
120-621. Given distribution as shown in TID-4500 (16th ed.) under Metals, Ceramics, and Materials category